Computational Methods for Astroparticle Propagation

Rafael Alves Batista

September 1, 2023

This course is designed to provide an introduction to the computational methods used to model the propagation of high-energy cosmic messengers, namely cosmic rays, gamma rays, and neutrinos. Students will learn about the physical processes that govern the propagation of these particles, as well as the techniques used to describe their transport in astrophysical environments. Topics will include the theory of astroparticle transport, the computational techniques commonly employed, and specific codes used by the community. Also discussed will be the limitations of model-building and the role of uncertainties in interpreting the results.

Warning: These notes are incomplete and will be updated over time. There most likely are many typos and a few errors. Be careful when using them!

Contents

1 Introduction

We are now at a unique moment to study the universe using all observational windows available. Low-energy ($E \lesssim 10^{15}$ eV) cosmic rays are being used to further constrain dark matter properties with experiments such as the Alpha Magnetic Spectrometer [**?**]. High- (10^{15} eV $\lesssim E \lesssim 10^{18}$ eV) and ultra-high-energy cosmic rays (UHECRs), with $E \gtrsim 10^{18}$ eV, have given us a glimpse into the mechanisms whereby particles are accelerated to energies well beyond the capabilities of particle accelerators such as the Large Hadron Collider, providing further insights into the most extreme processes in Nature [**?**]. The IceCube Neutrino Observatory has detected dozens of high-energy neutrinos unassociated to any known sources [**?**], and few in probable coincidence with astrophysical objects [**?**]. Imaging air Cherenkov telescopes such as MAGIC, H.E.S.S., and VERITAS have discovered hundreds of sources of very-high-energy gamma rays ($E \gtrsim 1$ TeV) both in the Galaxy and outside of it [**?**]. With the recent findings by LIGO we have witnessed the dawn of gravitational-wave astronomy [**?**].

To make sense of observations of this ecosystem of extreme cosmic accelerators shining bright through the lenses of various messengers, it is important to understand how they travel to Earth, which other particles they leave in their wake, and the countless obstacles they face during their journey. This is the purpose of the course on ***Computational Methods for Astroparticle Propagation*** – possibly the first of its kind.

This *preliminary* set of lecture notes I attempt to condense much of what has to be considered when *modelling* the transport of high-energy particles in the universe, namely cosmic rays (CRs), gamma rays, and neutrinos.

I present the relevant theoretical background in §2. Computational methods for treating the phenomena of interest considering this theoretical background are described in §3. In §4 a well-known tool to model the propagation of high-energy astroparticles is described, the CRPropa code.

Throughout this text I try to stick with S.I. units[1], since Gaussian units are an aesthetic abomination. I also attempt to perform calculations within the framework of special relativity (SR), as it is more generic, deriving the non-relativistic cases from these more generic results. For pedagogical reasons I also opt for "unnatural units", writing Planck's constant and speed of light explicitly everywhere.

---

[1]This is motivated by the fact that in electromagnetism Gaussian units are not rationalised, removing 4π factors from where they belong (like Coulomb's law). While Gaussian units sometimes make the equations look simpler, the degree of confusion it causes should have made people abandon it altogether. I failt to see how this has not yet happened.

2 The theory of particle propagation

Some particles do not propagate in a straightforward manner. In certain environments, they can be considerably influenced by external factors such as magnetic fields or interactions with other particles. These settings encompass intergalactic space, the vicinity of astrophysical objects, our own galaxy, and even Earth's atmosphere. The fundamental principles that describe these processes remain consistent, regardless of the specific environment in which they take place. This section provides a comprehensive overview of some of these principles, which are relevant for the propagation of high-energy astroparticles.

2.1 Basic concepts

To describe how particles propagate, one ought to bear in mind that this process is often stochastic in nature. Therefore, it is convenient to consider a collection of N identical particles and perform a statistical treatment.
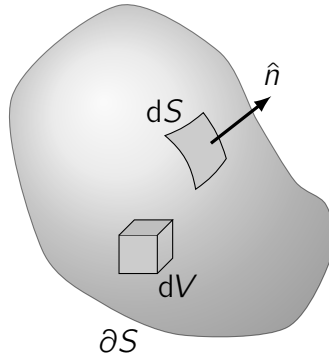
Figure 1: Illustration of an arbitrary volume with boundary ∂S. The area element is $\mathrm{d}\vec{S} \equiv \mathrm{d}S\hat{n}$, where $\hat{n}$ is the unit vector normal to this element, and $\mathrm{d}V$ is the volume element.

Consider an arbitrary surface S with boundary labelled ∂S, as shown in figure 1. An infinitesimally small arbitrary volume element of S is represented by $\mathrm{d}V$. Similarly, the corresponding area element is $\mathrm{d}\vec{S} = \mathrm{d}S\hat{n}$, wherein $\hat{n}$ is the unit vector normal to this surface. In the following sections some notions building up on these geometrical considerations are discussed, in particular the concept of *flux*.

2.1.1 Particle fluxes

The **directional flux** (ϕ) crossing the surface S at direction $\hat{\varrho}$ is defined as the number of particles (N) crossing the surface boundary ∂S, per unit time (t), per unit solid angle (Ω):

$$\phi\left(t, \hat{\varrho}\right) = \frac{\mathrm{d}^3 N}{\mathrm{d}t\,\mathrm{d}S\,\mathrm{d}\Omega}\,. \tag{1}$$

Note that the direction ($\hat{\varrho}$) is directly related to the solid angle. In fact, the solid angle element ($\mathrm{d}\Omega$) subtended by the surface element $\mathrm{d}S$ along the direction $\hat{\varrho}$ at a distance r is defined as

$$\mathrm{d}\Omega = \mathrm{d}S\left(\hat{n} \cdot \hat{\varrho}\right)\frac{1}{r^2}\,. \tag{2}$$

The **total flux** (Φ), or simply **flux**, is the surface-integrated flux crossing a surface:

$$\Phi(t) = \iint\limits_S \mathrm{d}\Omega\, \phi(t, \hat{\varrho}) \,. \tag{3}$$

From eqs. 1 and 3 it is possible to defined the corresponding energy-dependent fluxes. The **directional spectral flux** (j) at an instant t is

$$\mathrm{j}(t, \hat{\varrho}, E) = \frac{\mathrm{d}\phi(t, \hat{\varrho})}{\mathrm{d}E} = \frac{\mathrm{d}^4 N}{\mathrm{d}t\,\mathrm{d}S\,\mathrm{d}\Omega\,\mathrm{d}E} \,. \tag{4}$$

Similarly, the **spectral flux** (j) crossing the surface S can be written as

$$j(t, E) = \frac{\mathrm{d}\Phi(t)}{\mathrm{d}E} \,. \tag{5}$$

The **number density** of a distribution of particles is defined as

$$n(\vec{r}) = \frac{\mathrm{d}^3 N}{\mathrm{d}\vec{r}} = \frac{\mathrm{d}N}{\mathrm{d}V} = \frac{\mathrm{d}N}{\mathrm{d}r\,\mathrm{d}S} \,. \tag{6}$$

If the particles are moving with constant velocity $\vec{v}$, then this equation reduces to

$$n(t) = \frac{\mathrm{d}^2 N}{v\mathrm{d}t\,\mathrm{d}S} \equiv \frac{1}{v}\Phi \,. \tag{7}$$

2.1.2 Cross sections

A generic process $a + b \rightarrow f$ characterises **elastic scattering** if the final state (f) is composed by the same initial particles (a and b) and no other, which simply means they exchanged momentum among themselves. In **inelastic scattering** the particles a and b are not necessarily part of the final state f.

The **total cross section** (σ_{tot}) is defined as the sum of the cross sections for elastic (σ_{ela}) and inelastic scattering (σ_{ine}):

$$\sigma_{\text{tot}} = \sigma_{\text{ela}} + \sigma_{\text{ine}} \,. \tag{8}$$

Inelastic scattering lead, by definition, to the creation of secondary particles (c): $a + b \rightarrow c + \dots$. The **inclusive cross section** describes exactly this reaction, ignoring all other channels such as $a + b \rightarrow d + \dots$, and so on. In contrast, **exclusive cross sections** include all possible by-products of the interaction: $a + b \rightarrow c + d + \dots$.

Inheriting from the mathematical formalism commonly employed in accelerator physics, it is convenient to consider the laboratory frame. In this frame the notation $i + t \rightarrow f$ is simpler, wherein i refers to the incident particles and t denotes the target; f still denotes an arbitrary final state, as before. Now the cross section for this process can be defined as [**?**]

$$\sigma_{i+j\rightarrow f} = \frac{1}{\Phi_i} \frac{\mathrm{d}N_f}{\mathrm{d}t} \,, \tag{9}$$

where Φ_i is defined as in eq. 3. The final state can take various values for the momentum ($\vec{p}_f$). This

is captured by the **differential cross section**:

$$\frac{\mathrm{d}^3\sigma_{i+j\to f}}{\mathrm{d}^3\vec{p}_f} = \frac{1}{\Phi_i}\frac{\mathrm{d}^4 N_f}{\mathrm{d}^3\vec{p}_f\,\mathrm{d}t}\ . \tag{10}$$

Here the cross section is *inclusive*. The exclusive cross section for a process $i + t \to f_1 + f_2 + \ldots + f_j$, where j denotes the number of secondaries, can be written by a generalisation of the equation above:

$$\frac{\mathrm{d}^3\sigma_{i+j\to f_1+\ldots+f_j}}{\mathrm{d}^3\vec{p}_f} = \frac{1}{\Phi_i}\frac{\mathrm{d}^{3j+1} N_f}{\mathrm{d}^3\vec{p}_{f_1}\,\ldots\,\mathrm{d}^3\vec{p}_{f_j}\,\mathrm{d}t}\ . \tag{11}$$

2.2 Interaction lengths

Now the problem at hand consists in finding out what is the probability that a particle will interact after a given distance, considering the presence of targets that represent other particles. Classically, considering a collection of target particles at rest in the laboratory frame, this probability is related to the notion of **cross section** (σ), which takes into account the amount of "free space" in a target that would allow for an incident particle to cross. Therefore, the classical notion is purely geometrical, similar to what was originally described by Ernest Rutherford in his well-known 1911 experiment [**?**].

The classical notion of cross section has to be abandoned when treating quantum scattering. Moreover, particles might not be all static, which makes the treatment more intricate. Henceforth I will employ this broader definition, despite the fact that I will present a seemingly "semi-classical" approach to formulate the problem and obtain a general solution.

The goal is to compute the **interaction length** (λ) of a single particle with a target composed of multiple particles after moving a distance $r \equiv |\vec{r}|$ in the region where the targets are located, bounded by a surface S (see figure 1). Essentially, this process can be written as $i + t \to f$, where, again, 'i' refers to the incident particles, 't' denotes the target particles, and 'f' is a generic final state. The infinitesimal displacement vector $\mathrm{d}\vec{r}$ can be written as $\mathrm{d}\vec{r} = \vec{v}\mathrm{d}t$. The directional unit vector $\hat{r} = \vec{r}/|\vec{r}|$ can be decomposed into two components, a radial ($\hat{\varrho}$) and a directional ($\hat{\theta}$) one: $\hat{r} \equiv \hat{\varrho} + \hat{\theta}$. Under the assumption of spherical symmetry, this simplifies to $\mathrm{d}r = v\mathrm{d}t$ and $\hat{r} = \hat{\varrho}$.

For simplicity, assume first that the incident particles are bundled together, all moving with the same constant velocity ($\vec{v}$), parallel to each other. This establishes a relationship between the distance travelled (r) and time (t): $\vec{v} = \vec{r}/t$. Since the velocity is constant (by hypothesis), then $\mathrm{d}\vec{r} = \vec{v}\mathrm{d}t$. The incident particle crosses the boundary ∂S and travel an infinitesimally tiny distance $\mathrm{d}r \equiv \mathrm{d}|\vec{r}| = v\mathrm{d}t$ inside the volume defined by the surface S.

Consider the interaction between the incident and target particles: *what fraction of the incident particles will undergo interactions with the target particles within this volume?* To answer this question, the notion of cross section (σ) is once again needed. An interplay between the number density of target particles (n_t) and the characteristic length for interactions between the incident and target particles (λ) defines the cross section: $\sigma = (n_\mathrm{t}\lambda)^{-1}$. Note that this expression does *not* provide the cross section for interactions between two particles. That comes from particle physics considerations. In reality, it would be more appropriate to write it as $\lambda = (n_\mathrm{t}\sigma)^{-1}$, since the interaction length (λ) is the quantity actually being calculated here.

For the generic process $i + t \rightarrow f$, the spectral flux of incident particles (j_i) will change by dj_i

$$\frac{dj_i(E)}{dr} = -n_t \sigma_{i+t \rightarrow f}(E_i, E_t) j_i(E) = -\lambda(E_i, E_f) j_i(E_i) = \phi_f(E_f). \tag{12}$$

Note the negative sign, which indicates that the incident flux is *attenuated* due to interactions with the target. This equation, however, is oversimplified. The target number density can be energy-dependent, and the cross section can be a function of *both* the incident and target energies and the geometry. This implies $n_t = n_t(E_t)$ and $\sigma = \sigma(E_t, E_i, y)$, wherein y denotes the fraction of the primary's energy retained after the scattering. This can be written as

$$\frac{d\phi(E)}{dr} = -\int_0^\infty \int_0^\infty \int_0^1 dE_t dE_i dy \, n(E_i) \, \sigma(E_t, E_i, y) \phi(E_i). \tag{13}$$

2.3 Kinematics of two-body interactions

The interaction between two particles can be modelled within the framework of (special-)relativistic kinematics.

Consider an interaction between any two particles '1' and '2' with masses m_1 and m_2, respectively. Their four-vectors are $P_1 = (E_1/c, \vec{p}_1)$ and $P_2 = (E_2/c, \vec{p}_2)$, wherein E denotes the energy and $\vec{p}$ the momentum in the *laboratory frame*.

The squared centre-of-mass energy ($s \equiv E_{CM}^2$) is a relativistic invariant. For the centre-of-mass, this invariant reads

$$s = E_{CM}^2 = (E_1 + E_2)^2 - (\vec{p}_1 + \vec{p}_2)^2 c^2, \tag{14}$$

which reduces to

$$s = m_1^2 c^4 + m_2^2 c^4 + 2E_1 E_2 (1 - \beta_1 \beta_2 \cos\theta). \tag{15}$$

Here $\beta \equiv v/c$ refers to the speed of the particle, and θ is the angle (in the lab frame) between the two particles.

A remarkable feature of equation 15 is that it does not depend on the outcomes of the process of interest. It can be used generically for any two particles.

2.4 Targets for interactions

2.4.1 Cosmological radiation fields

The universe is permeated with radiation covering a wide frequency range of the electromagnetic spectrum. This radiation may be the integrated diffuse signal resulting from structure formation processes, like the extragalactic background light (EBL) and the cosmic radio background (CRB), or a relic of some primeval process, as the cosmic microwave background (CMB). These three backgrounds are the most important ones when it comes to modelling the propagation of astroparticles over cosmological distances.

A general overview of the energy density of the different backgrounds is shown in figure 2. Note that, while this figure refers to redshift $z = 0$, these models can differ considerably at higher redshifts.

There are other radiation fields that may impact particle propagation. For instance, in the Milky Way the interstellar radiation field (ISRF) plays an important role for the propagation of Galactic
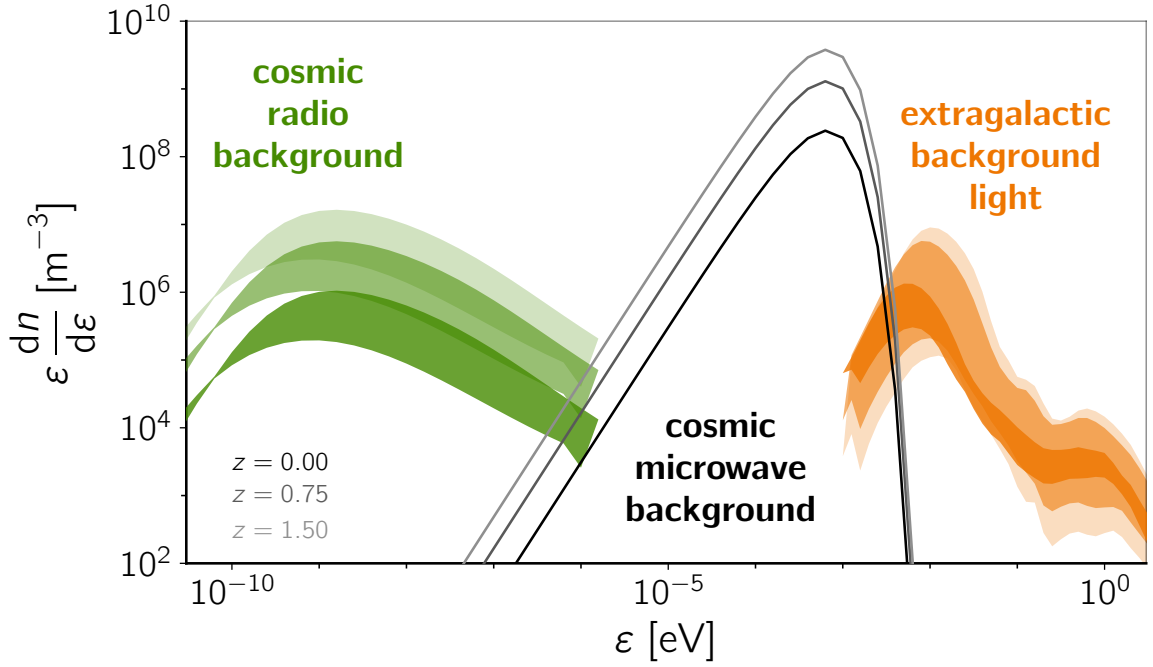
Figure 2: Spectral number density of photons for different backgrounds: CMB (dotted), EBL (solid), and CRB (dashed lines). Different colours indicate the different backgrounds. Bandas encompass several models for the CRB [**? ? ?**] and for the EBL [**? ? ? ? ?**].

cosmic rays (GCRs) and very energetic photons.

2.4.1.1 Cosmic microwave background (CMB)

The CMB is the most well-understood among the extragalactic diffuse radiation backgrounds. It is a black body of temperature T_{cmb} with energy density

$$\frac{\mathrm{d}n(\varepsilon)}{\mathrm{d}\varepsilon} = \frac{\varepsilon^2}{\pi^2 c^3 \hbar^2} \frac{(1+z)^2}{\exp\left(\frac{\varepsilon}{k_B T_{\text{cmb}}}\right) - 1} \tag{16}$$

where ε is the photon energy, k_B is Boltzmann's constant, and T_{cmb} the CMB temperature. The temperature evolves with redshift (z) as

$$T_{\text{cmb}}(z) = T_{\text{cmb}}(0)\,(1+z)\,, \tag{17}$$

where $T_{\text{cmb}}(0) \approx 2.73$ K [**?**]. The density of CMB photons today is $\simeq 4 \times 10^8$ m^{-3}.

2.4.1.2 Extragalactic background light (EBL)

The EBL encompasses electromagnetic radiation ranging from infrared to ultraviolet. Unlike the CMB, which evolved virtually undisturbed since the matter-radiation decoupling in the early Universe, the EBL is affected by several processes, in particular, energy released during structure formation. In fact, it is fair to view it as a calorimeter of sorts, since it results from the energy released into the IGM throughout cosmic history, especially at early times, with absorption by dust and subsequent

8

re-emission at longer wavelengths [? ? ?].

Given its importance for understanding structure formation [?], as well as for gamma-ray [? ?] and UHECR propagation [? ?], new EBL models are constantly being developed [? ? ? ? ? ? ? ? ?].

At optical wavelengths, the diffuse background is poorly known due to intrinsic difficulties in removing foregrounds such as Galactic emission and zodiacal light (see, e.g., [? ?] for in-depth discussions). There are some measurements of the optical background [? ?], but the most reliable results were delivered by probes in the outer Solar System [? ? ?]. The integrated contribution of the light emitted by galaxies and stars, as well as by extragalactic gas, respond for a significant fraction of this flux. Nevertheless, a part of it remains unexplained [? ?].

Some EBL models encompass part of the ultraviolet region of the electromagnetic spectrum, which is at the threshold of what is physically relevant for understanding how astroparticles propagate. This emission can be attributed in part to dust-scattered light emitted by hot objects (for reviews, see refs. [? ?]). However, this mechanism does not respond for all of the measured ultraviolet background, and the debate is ongoing [? ? ? ? ?].

2.4.1.3 Cosmic radio background (CRB)

The CRB is an important ingredient to model the propagation of ultra-high energy (UHE) particles, despite being often overlooked. For reviews, the reader is referred to, e.g., refs. [? ? ?]. It is mostly dominated by radio emission from normal, radio, and starburst galaxies [? ?]. Observations by ARCADE2 [?] revealed an unexpected excess in this background, at frequencies between 22 MHz and 10 GHz, which does not fit the previous picture. A number of interpretations for this anomaly were suggested [? ? ? ? ?] (but see [? ?]). CRB models commonly used to study the propagation of UHE particles include the one by Protheroe & Biermann [?], recently updated by Niţu *et al.* [?].

2.5 Magnetic fields

Magnetic fields are an essential ingredient to make sense of astrophysical observations of high-energy particles, especially in the multimessenger context. For this reason, this section provides a somewhat detailed description of them.

The properties of cosmic magnetic fields across the universe can be very different depending on where they are located. Nevertheless, the fact is that they are truly ubiquitous, being present everywhere. They can be regular or stochastic in different environments. While the former is easier to be grasped intuitively, the later requires some mathematical formalism, introduced in §2.5.1. Sections §2.5.2 and §2.5.3 briefly describe the properties of these fields at intergalactic and Galactic scales, respectively. The detailed description of the motion of charged particles in magnetic fields is provided in §2.5.4.

2.5.1 Characterisation of stochastic magnetic fields

Stochastic magnetic fields are characterised by the associated probability distribution functions of a field $\vec{B}$. They can be described by means of statistical averages of the relevant observables. They are often modelled as a zero-mean Gaussian random field, which are the ones considered hereafter.

The average strength ($B = |\vec{B}|$) of a stochastic magnetic field is $\left\langle |\vec{B}| \right\rangle = 0$. This is a reasonable approximation considering the *cosmological principle*, which posits that the Universe is homogeneous

and isotropic at very large scales. As a consequence, all individual components of the magnetic field would average to zero ($\langle B_x \rangle = \langle B_y \rangle = \langle B_z \rangle = 0$), under the typical assumption that they are normally distributed – a reasonable first-order approximation.

When one refers to the *strength* of stochastic magnetic fields, often what is meant is not the average field within a given volume V, but its root mean square (RMS) value[2]:

$$B^2 \equiv B_{\text{rms}}^2 = \frac{1}{V} \int_V \mathrm{d}^3 \vec{r}\, \vec{B}(\vec{r}) \cdot \vec{B}(\vec{r})\,. \tag{18}$$

Magnetic-field lines can have non-trivial topologies, whose information is encoded in a quantity called **magnetic helicity** (H_B), defined as:

$$H_B = \frac{1}{V} \int_V \mathrm{d}^3 \vec{r}\, \vec{B}(\vec{r}) \cdot \vec{A}(\vec{r})\,, \tag{19}$$

with $\vec{A}$ denoting the magnetic vector potential, whose curl equates the magnetic field ($\vec{B} = \vec{\nabla} \times \vec{A}$). This quantity is important in cosmology because it relates to many processes taking place in the early Universe like baryogenesis and leptogenesis [?], in addition to playing a role in the evolution of the magnetic field itself and consequently in the formation of structures [?].

Stochastic magnetic fields are usually described by their Fourier representation:

$$\tilde{\vec{B}}\left(\vec{k}\right) = \frac{1}{(2\pi)^{3/2}} \int_V \mathrm{d}^3 \vec{r}\, \vec{B}(\vec{r}) e^{-i\vec{k}\cdot\vec{r}}\,, \tag{20}$$

with $\vec{k}$ representing the wave vector. This choice of representation is useful because it enables a simplified description of the correlation between any two modes $\vec{k}$ and $\vec{k}'$. For instance, for two spatial coordinates a and b, the ensemble average of the magnetic field is

$$\left\langle \tilde{B}_a(\vec{k}) \tilde{B}_b(\vec{k}') \right\rangle = (2\pi)^3\, \delta^{(3)}(\vec{k} - \vec{k}') \mathcal{P}_{ab}(\vec{k}')\,. \tag{21}$$

For a homogeneous and isotropic magnetic field, $\mathcal{P}_{ab}$ is given by

$$\mathcal{P}_{ab}(\vec{k}) = \frac{\mathcal{P}_0}{k^2} \left[\left(\delta_{ab} - \frac{k_a k_b}{k^2} \right) M(\vec{k}) + \frac{i}{c_H} \epsilon_{abc} k_c \mathcal{H}(\vec{k}) \right]\,, \tag{22}$$

where ϵ_{abc} is the Levi-Civita symbol, δ_{ab} is the Kronecker delta, $\mathcal{P}_0$ is a normalisation constant, $\mathcal{H}(\vec{k})$ is the spectral density of magnetic helicity, c_H is a constant, and $k \equiv |\vec{k}|$ is the absolute value of the wave vector. The spectral magnetic energy ($M(\vec{k})$) is linked to $\mathcal{H}(\vec{k})$ via the relation

$$|\mathcal{H}| \leq \frac{|c_H|}{k} M\,. \tag{23}$$

Note that it is through the correlator (eq. 22) that the magnetic power spectrum (M) comes into play. It is assumed to follow a power law of the form

$$M(\vec{k}) \propto |\vec{k}|^{\alpha_B - 1} \propto k^2 \left| \tilde{\vec{B}}(\vec{k}) \right|\,, \tag{24}$$

---

[2]This is, indeed, a very common misconception that pervades the literature, especially works on UHECRs.

where α_B is the spectral index of the magnetic field. At present time, for large values of k, i.e., for small scales, cosmological magnetic fields are thought to be of Kolmogorov-type ($\alpha_B = -2/3$) [? ?] or Iroshnikov–Kraichnan–type ($\alpha_B = -1/2$) [? ?]. At larger scales, $\alpha_B = 5$ (Batchelor spectrum) is expected. Moreover, if magnetic fields originated during inflation, its spectrum would most likely be scale-invariant ($\alpha_B = 0$) [? ? ? ?].

The last relevant statistical observable is the **correlation length** or **coherence length** (L_B), which relates to the dominant scale of the magnetic field, i.e., the average size of the eddies. It can be written as [?]

$$L_B = 2\pi \frac{\int \mathrm{d}k\, k^{-1} M(\vec{k})}{\int \mathrm{d}k\, M(\vec{k})} \, . \tag{25}$$

Several other definitions can be found in the literature [? ?].

A magnetic turbulence description frequently found is the cascade model (e.g. [? ? ?]), wherein magnetic energy is injected at large scales (the so-called *energy range*) and subsequently transferred to smaller scales (the *inertial range*), below which the turbulent energy tends to dissipate.

Turbulent stochastic magnetic fields tend to follow power laws of the form of eq. 24. This is supported by observations of interplanetary and interstellar magnetic fields [? ? ?]. In practice, eq. 24 does not cover an infinitude of k's, being restricted to values of larger than a given cut-off wave number (i.e., $k \geq k_0$) and vanishing outside this range.

2.5.2 Intergalactic magnetic fields

All charged particles coming from astrophysical objects outside the Milky Way can have their trajectories influenced by **intergalactic magnetic fields (IGMFs)**. Our current knowledge of IGMFs is poor. This limitation is partly attributed to the gap in understanding their origin and evolution (for comprehensive reviews, see [? ?]).

IGMFs are believed to permeate the universe at large scales. Inside galaxy clusters, they can attain intensities of about $\sim 10^{-10}$ T in the central regions [? ?]. In the large-scale filaments connecting by cluster, their strength lies between $\sim 10^{-12}$ and 10^{-11} T [? ?]. The scenario within cosmic voids remains less clear. Within these regions' inner parts, IGMFs might not exist at all if their origins were tied to spatially localised astrophysical processes. Nonetheless, gamma-ray observations impose lower limits on integrated IGMFs along the line of sight, predominantly influenced by voids, indicating values of $B \gtrsim 10^{-21}$–10^{-19} T [? ? ? ? ? ? ?].

Uncertainties related to IGMFs in cosmic voids are even more relevant when considering that these voids constitute a substantial portion of the universe's volume, ranging from about 20% to 80%. The remainder of the volume is filled by galaxy clusters and filaments, with the clusters accounting for merely $\lesssim 10^{-3}$ [? ?]. This discrepancy emphasises that charged particles journeying cosmological distances are likely to be influenced by the fields prevailing in voids.

The typical size of the magnetic domain, this is, the coherence length (L_B), remains even more uncertain. If they are very large, this might not be an issue, but given the vast parameter space, there is no reason to believe this might be the case. In the context of filaments and galaxy clusters, these fields tend to be bound by the size of these structures. However, within voids, their range spans a diverse spectrum, varying from a fraction of a parsec to dimensions encompassing the observable universe [? ?]. Current constraints on the coherence scale are weak, but there is some support for $10\,\text{kpc} \lesssim L_B \lesssim 100\,\text{Mpc}$ [?].

The helicity of IGMFs have also been suggested to affect the propagation of charged particles in
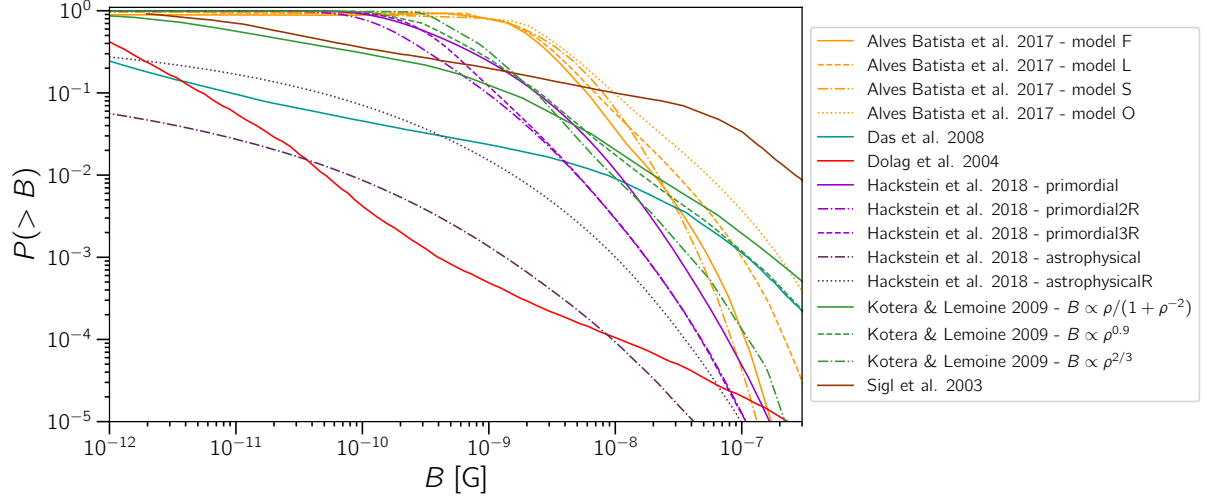
Figure 3: Comparison of the cumulative volume filling factors according to various studies [? ? ? ?]. Figure taken from ref. [?].

magnetic fields [? ? ?], which could have profound implications for understanding early-universe cosmology (see, e.g., ref. [?] for a review).

Investigations of the motion of charged particles in the magnetised cosmic web primarily hinge on cosmological N-body simulations. In these simulations, a designated volume evolves from its inception to the current state through magnetohydrodynamics (MHD). Nevertheless, there exists disparities among different simulations (e.g. [? ? ? ? ?]), in particular in their filling factors, which describe the fraction of the universe's volume with fields stronger than a given value of reference. A compilation of some of these models is shown in fig. 3.

2.5.3 Galactic magnetic fields

The study of the Galactic magnetic field (GMF) is remarkably challenging (see, e.g., ref. [? ?] for a review). Drawing from the available observational data, an array of GMFs has emerged, each capable of fitting specific datasets. Nevertheless, inherent degeneracies among these models persist [? ? ?].

Within the disc, the Galaxy's field is believed to be an axisymmetric spiral with strength $\sim$ 0.6 nT [? ?]. The pitch angle of this spiral is, however, uncertain [? ?]. Driving the total field strength, the turbulent component exhibits considerable variability. Its coherence length spans from scales as small as parsecs up to ~ 1 kpc [?]. Interestingly, the coherent component of the field reverses several times at scales larger than this, in the middle of the Galactic plane [?].

Several models for the GMF exist. While the earlier ones were analytical, only in the last two decades has it been possible to build all-encompassing models based on a variety of observational tracers, such as the widely-used Jansson & Farrar [? ?]. With the growing body of observations, this model is being revisited and will likely be improved in the near future [? ?].

2.5.4 Propagation of charged particles

The momentum ($\vec{p}$) of a charged particle of charge q and mass m propagating with velocity $\vec{v} = \vec{p}/\gamma m$ in a magnetised media can change according to the Lorentz force ($\vec{F}_B$), given by

$$\vec{F}_B\,(\vec{r}, t) = \frac{\mathrm{d}\vec{p}\,(\vec{r}, t)}{\mathrm{d}t} = m\frac{\mathrm{d}\vec{v}\,(t)}{\mathrm{d}t} = q\left(\vec{E}\,(\vec{r}, t) + \vec{v}(t) \times \vec{B}\,(\vec{r}, t)\right) \tag{26}$$

where $\vec{r}$ is the position of the particle, t the time in some convenient coordinate system, and γ represents the Lorentz factor of the particle. Here $\vec{E}$ and $\vec{B}$ denote, respectively, the electric and magnetic fields of the medium. In many astrophysical applications $|\vec{E}| \approx 0$[3].

Eq. 26 can be written in terms of the velocity, instead of the momentum, resulting in

$$\frac{\mathrm{d}\vec{v}(t)}{\mathrm{d}t} = \frac{q}{\gamma m}\vec{v}(t) \times \vec{B}\,(\vec{r}, t) \ . \tag{27}$$

Together with

$$\vec{v} = \frac{\mathrm{d}\vec{r}}{\mathrm{d}t}\,, \tag{28}$$

eq. 27 constitute a set of differential equations whose solution fully describes the motion of the particle under the influence of the magnetic field ($\vec{B}$).

2.5.4.1 A homogenous magnetic field

To solve the equations of motion of a charged particle in a magnetic field, consider first the case of a homogeneous magnetic field: $\vec{B}\,(\vec{r}, t) = \vec{B}$. Without loss of generality, a coordinate system can be chosen oriented along the z axis: $\vec{B} = B\hat{z}$. In this case, the velocity component of $\vec{v}$ parallel to $\hat{z}$ is completely arbitrary and irrelevant for propagation because of the vector product $\vec{v} \times \vec{B}$. This reduces the complexity of the problem by making the treatment of one of the dimensions trivial. The solution to the equations of motion can be obtained by solving a system of two differential equations of first order in the velocity:

$$\begin{cases} \dfrac{\mathrm{d}v_x}{\mathrm{d}t} = \dfrac{q}{m\gamma}Bv_y & \equiv \omega v_y \\[2mm] \dfrac{\mathrm{d}v_y}{\mathrm{d}t} = -\dfrac{q}{m\gamma}Bv_x & \equiv -\omega v_x \\[2mm] \dfrac{\mathrm{d}v_z}{\mathrm{d}t} = 0 & \end{cases} \tag{29}$$

To simplify the notation, the **gyrofrequency** is defined:

$$\omega \equiv \frac{|q|B}{m\gamma} \ . \tag{30}$$

In addition, the parallel and the perpedincular components of the velocity with respect to the magnetic field are introduced: $\vec{v}_\parallel(t) \equiv v_z(t)\hat{z}$ and $\vec{v}_\perp(t) \equiv v_x(t)\hat{x} + v_y(t)\hat{y}$.

In general, $\vec{v}(t) = \vec{v}_\parallel(t) + \vec{v}_\perp(t)$, but in this particular case these quantities are all constant ($|\vec{v}_\parallel + \vec{v}_\perp| = |\vec{v}| = $ constant). A useful concept that can be introduced at this stage is the **pitch**

---

[3]This assertion can be proven by demonstrating the existence of another reference frame where the electric field $\vec{E}$ is null, by performing a Lorentz transformation. This follows immediately from the principle of relativity, which states that all non-inertial frames are equivalent, such that the rest frame of the particle in motion can be chosen.

angle, ϕ_p, which links the parallel and perpendicular components of the velocity as follows:

$$\tan \phi_p(t) = \frac{v_\perp(t)}{v_\parallel(t)} \, . \tag{31}$$

For the simple homogeneous magnetic field considered here, the pitch angle is constant. This follows from the fact that $\frac{dv_\parallel}{dt} = 0$, which implies $\frac{dv_\perp}{dt} = 0$.

The solution to the system of differential equations is immediate:

$$v_x(t) = v_\perp \cos(\varphi - \omega t) \, , \tag{32}$$
$$v_y(t) = v_\perp \sin(\varphi - \omega t) \, , \tag{33}$$
$$v_z(t) = v_\parallel \, , \tag{34}$$

where φ is a phase factor. To obtain the time-dependence of the coordinates, these equations should be integrated, yielding

$$x(t) = x(0) + \frac{v_\perp}{\omega} \sin \varphi - \frac{v_\perp}{\omega} \sin(\varphi - \omega t) \, , \tag{35}$$
$$y(t) = y(0) - \frac{v_\perp}{\omega} \cos \varphi + \frac{v_\perp}{\omega} \cos(\varphi - \omega t) \, , \tag{36}$$
$$z(t) = z(0) + v_\parallel t \, . \tag{37}$$

An example of how these results affect the trajectories of charged particles can be seen in figure 4.
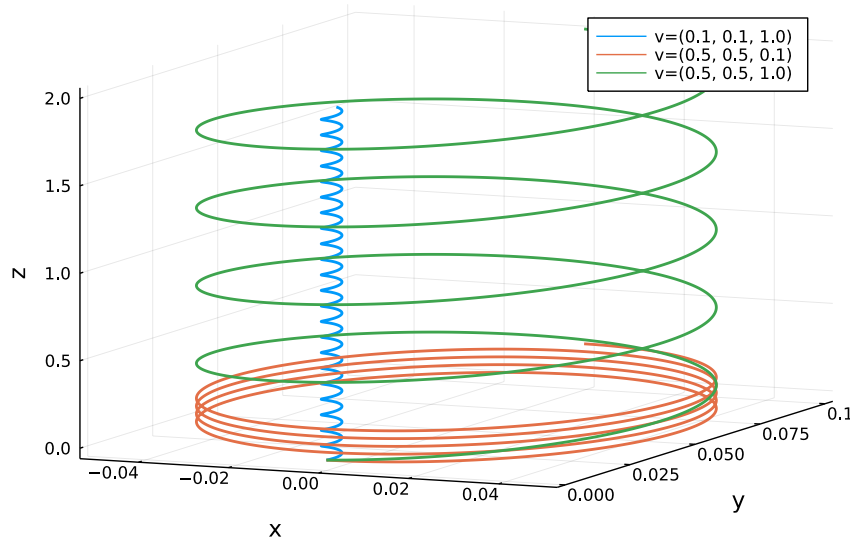
Figure 4: An example of the trajectory described by a particle in 3D. The parameters are arbitrary, except for the velocities. The different velocities are instructive to illustrate how the different combinations of perpendicular and parallel components affect the results.

Note that $v_x^2(t) + v_y^2(t) = \text{constant}$, which is a circular motion in the xy plane around the point

$$(x_{\text{centre}}, y_{\text{centre}}) = \left(x(0) + \frac{v_\perp}{\omega} \sin \phi, \, y(0) - \frac{v_\perp}{\omega} \cos \phi \right) \, . \tag{38}$$

It is possible to identify a characteristic quantity with dimensions of length related to the gyrofre-

quency. This is the **Larmor radius** (or **gyroradius**), given by

$$R_L = \frac{v_\perp}{\omega} = \frac{\gamma m v_\perp}{|q|B} \, .$$ (39)

In the ultrarelativistic limit, assuming small pitch angles ($\tan\phi_p \approx 0$) such that $v_\parallel \gg v_\perp$ (see eq. 31), $v_\parallel \approx c$. In this case, the usual relativistic dispersion relation becomes

$$E^2 = (pc)^2 + \left(mc^2\right)^2 = c^2\left(p_\perp + p_\parallel\right)^2 + \left(mc^2\right)^2 \approx p_\parallel^2 c^2 \, .$$ (40)

Therefore, the definition of the Larmor radius (eq. 39) can be rewritten in a more convenient form in terms of the energy $E = \gamma mc^2$ of the particle:

$$R_L = \frac{E}{|q|cB} \, .$$ (41)

2.5.4.2 A homogenous magnetic field with a perturbation

Suppose a perturbation ($\delta\vec{B}$) is added to the simple magnetic field from §2.5.4.1, now denoted $\vec{B}_0$ (with $B_0 \equiv |\vec{B}_0|$), which can be in an arbitrary direction. The total field now reads $\vec{B} = \vec{B}_0 + \delta\vec{B} = B_0\hat{z} + \delta\vec{B}$. This can be plugged into the equation of motion (eq. 27):

$$\frac{\mathrm{d}\vec{v}}{\mathrm{d}t} = \frac{q}{m\gamma}\vec{v}\times\vec{B} = \frac{q}{\gamma m}\vec{v}\times\vec{B}_0 + \frac{q}{\gamma m}\vec{v}\times\delta\vec{B} \, .$$ (42)

The solution for first term on the right-hand side of the last equality is known (eqs. 32–34 and 35–37). To obtain the full solution, one must first write down the system of differential equations:

$$\begin{cases} \dfrac{\mathrm{d}v_x}{\mathrm{d}t} = \omega_0\left(v_y\dfrac{\delta B_z}{B_0} - v_z\dfrac{\delta B_y}{B_0}\right) + \omega_0 v_y \, , \\[2mm] \dfrac{\mathrm{d}v_y}{\mathrm{d}t} = \omega_0\left(v_z\dfrac{\delta B_x}{B_0} - v_x\dfrac{\delta B_z}{B_0}\right) - \omega_0 v_x \, , \\[2mm] \dfrac{\mathrm{d}v_z}{\mathrm{d}t} = \omega_0\left(v_x\dfrac{\delta B_y}{B_0} - v_y\dfrac{\delta B_x}{B_0}\right) \, , \end{cases}$$ (43)

where ω_0 is what was formerly ω, this is, the gyrofrequency corresponding to the unperturbed magnetic field (eq. 30). Note that each i-th component of the perturbations is assumed to vary slowly with time, such that $\frac{\mathrm{d}\delta B_i}{\mathrm{d}t} \sim 0$.

The set of differential equations 43 can be solved using variation of parameters. For simplicity, let $a_i(t)$ be the terms within parentheses times ω_0. The ansatz is the following:

$$v_x(t) = g_1(t)\cos\omega_0 t + g_2(t)\sin\omega_0 t \, ,$$ (44)
$$v_y(t) = g_2(t)\cos\omega_0 t - g_1(t)\sin\omega_0 t \, ,$$ (45)

where $g_1(t)$ and $g_2(t)$ are two functions to be determined. By inspection, it is possible to show that

$$g_1(t) = \int_0^t dt' \left[a_y(t') \cos \omega_0 t' - a_x(t') \sin \omega_0 t' \right] ,$$ (46)

$$g_2(t) = \int_0^t dt' \left[a_y(t') \sin \omega_0 t' + a_x(t') \cos \omega_0 t' \right] .$$ (47)

After some tedious integrations (by parts), the velocities are obtained [**?**]:

$$v_x(t) = v_x(0) \cos \omega_0 t + v_y(0) \sin \omega_0 t + \cos \omega_0 t \int_0^t dt' \left[a_y(t') \cos \omega_0 t' - a_x(t') \sin \omega_0 t' \right]$$

$$+ \sin \omega_0 t \int_0^t dt' \left[a_y(t') \sin \omega_0 t' + a_x(t') \cos \omega_0 t' \right] ,$$ (48)

$$v_y(t) = v_y(0) \cos \omega_0 t - v_x(0) \sin \omega_0 t + \cos \omega_0 t \int_0^t dt' \left[a_y(t') \sin \omega_0 t' + a_x(t') \cos \omega_0 t' \right]$$

$$- \sin \omega_0 t \int_0^t dt' \left[a_y(t') \cos \omega_0 t' - a_x(t') \sin \omega_0 t' \right] .$$ (49)

The guiding centre follows the magnetic-field lines. The motion is a superposition of two components, one that rotates in the xy plane, and another that moves stochastically, as dictated by the perturbing field. For this reason, this is known as **perpendicular scattering**. A better understanding of this motion can be grasped by considering an arbitrary instant in time and integrating the velocities over one period:

$$u_i(t) = \frac{1}{T} \int_t^{t+T} dt' \, v_i(t') ,$$ (50)

where $T = 2\pi/\omega_0$ is the period of the particle. It follows then that

$$u_x(t) \approx \frac{1}{\omega_0} a_x(t) = v_z \frac{\delta B_x}{B_0} - v_x \frac{\delta B_z}{B_0} ,$$ (51)

$$u_y(t) \approx \frac{-1}{\omega_0} a_y(t) = v_z \frac{\delta B_y}{B_0} - v_y \frac{\delta B_z}{B_0} ,$$ (52)

$$u_z(t) \equiv v_z(t) .$$ (53)

Intermediate steps for this calculation are provided in ref. [**?**][4].

It is important to once again bring to the reader's attention the motivation for the description of a stochastic magnetic field in §2.5.1. The perturbation $\delta \vec{B}$ can be seen as the introduction of an additional turbulent field on top of an already-existing homogeneous one. This is essential for modelling how particles propagate in magnetic fields, since this exact treatment could be applied to determine particles' trajectories within individual magnetic domains with a regular (homogeneous)

---

[4]Note that here I employ S.I. units, whereas Shalchi [**?**] uses Gaussian cgs units. This introduces a few differences, in particular in the definition of the gyrofrequency.

component and a turbulent (perturbation) component on top of it, like in the Milky Way.

From here, it is only possible to obtain the position vector $\vec{r}(t)$ knowing properties of the perturbation ($\delta\vec{B}(\vec{r}, t)$), or statistically, for a collection of particles, as done in §2.5.4.3.

2.5.4.3 Ensemble propagation

Sections §2.5.4.1 covered the motion of a single charged particle in a homogeneous magnetic field. In §2.5.4.2 a perturbation was added to the magnetic field and a set of equations (eq. 43) was obtained. However, it was not directly solved because $\delta\vec{B}$ may be a function of position ($\vec{r}$) and time (t). Here the essential concepts of §2.5.1 are adopted. They serve as bases for the subsequent discussions. In particular, the relationship between the mean squared displacements ($\langle \Delta x^2 \rangle$, $\langle \Delta y^2 \rangle$, and $\langle \Delta z^2 \rangle$) and time, through the diffusion coefficient, will be used henceforth.

At this stage, a new concept comes in handy: the **running diffusion coefficient**, defined as:

$$d_{xx}(t) = \frac{1}{2}\frac{\mathrm{d}}{\mathrm{d}t}\left\langle \left(\Delta x(t)\right)^2 \right\rangle . \tag{54}$$

Here the coordinate 'x' is simply a placeholder for all cartesian coordinates, with $\Delta x \equiv x(t) - x(0)$.

Taking the limit of infinite time, the diffusion coefficiente κ_{xx} – which is a constant – corresponding to the running diffusion coefficient (d_{xx}) is obtained:

$$\kappa_{xx} = \lim_{t\to\infty} d_{xx}(t). \tag{55}$$

Nevertheless, it should be noted that this quantity is only mathematically defined as in reality time cannot be infinitely large. It suffices to employ d_{xx} to describe the system whenever $t \gg t_d$, i.e., when diffusive behaviour was reached after a time scale t_d.

These considerations show the importance of a *statistical* treatment of the relevant quantities, in particular the spatial coordinates. A useful mathematical toolkit to assist with these calculations is the Taylor-Green-Kubo (TGK) formalism.

When investigating the flow of Lagrangian particles, Taylor [?] came up with a simple and elegant way to describe statistical of a particle's displacement by using the velocity or, more specifically, the autocorrelation function thereof. Taylor's idea has been later revisited by Green [?] and Kubo [?] in the context of statistical mechanics. The **Taylor-Green-Kubo (TGK) approach**, as it became later known, is extremely useful to calculated diffusion coefficients to model the transport of an ensemble of particles in a given medium.

Eq. 53 imply that the charged particles will displace perpendicularly to the direction of the homogeneous field. The RMS of its displacement is given by

$$\left\langle \left(\Delta x(t)\right)^2 \right\rangle = \left\langle \left(\int_0^t \mathrm{d}t'\, v_x(t')\right)^2 \right\rangle , \tag{56}$$

which can be opened up as follows:

$$\left\langle \left(\Delta x(t)\right)^2 \right\rangle = \int_0^t \mathrm{d}t' \int_0^t \mathrm{d}t'' \left\langle v_x(t')v_x(t'') \right\rangle . \tag{57}$$

Note that the interval $[0, t]$ can be split into $[0, t']$ and $[t', t]$, such that

$$\left\langle (\Delta x(t))^2 \right\rangle = \int_0^t dt' \int_0^{t'} dt'' \left\langle v_x(t') v_x(t'') \right\rangle + \int_0^t dt' \int_{t'}^t dt'' \left\langle v_x(t') v_x(t'') \right\rangle . \qquad (58)$$

It is reasonable to assume homogeneity for most cases, such that $\langle v_x(t') v_x(t'') \rangle = \langle v_x(t' - t'') v_x(0) \rangle$ in the first integral, and $\langle v_x(t'' - t') v_x(0) \rangle$ in the second one. Therefore, it follows immediately from eq. 58 that

$$\left\langle (\Delta x(t))^2 \right\rangle = 2 \int_0^t dt' \, (t - t') \left\langle v_x(t') v_x(0) \right\rangle . \qquad (59)$$

For more details on this derivation, see section 1.3.2 of ref. [**?**] .

A process similar to that used to derive eq. 59 can also be employed to obtain other displacement correlators ($\langle \Delta x(t) \Delta z(t) \rangle$, $\langle \Delta z(t) \Delta z(t) \rangle$, etc), which might be required in more complex situations.

The running diffusion coefficient ($d_{xx}(t)$) can be obtained from eq. 59 by applying eq. 54, resulting in:

$$d_{xx}(t) = \int_0^t dt' \left\langle v_x(t') v_x(0) \right\rangle , \qquad (60)$$

which for fully diffusive propagation implies $d_{xx}(t \to \infty) = \kappa_{xx} = $ constant. This leads to **Kubo's equation**:

$$\kappa_{xx} = \int_0^\infty dt' \left\langle v_x(t') v_x(0) \right\rangle . \qquad (61)$$

Considering the other coordinates (y, and z), and the symmetry of the problem at hand — recall that this is fully motivated by the turbulent magnetic field case of §2.5.4.2 — it is possible to identify two diffusion coefficients, $d_{xx}(t) = d_{yy}(t) = d_\perp(t)$ and $d_{zz}(t) = d_\parallel(t)$ (and $\kappa_{xx} = \kappa_{yy} = \kappa_\perp$ and $\kappa_{zz} = \kappa_\parallel$). Therefore, two regimes are identified for the transport of charged particles, parallel and perpendicular. The diffusion coefficients ($\kappa_\parallel$ and $\kappa_\perp$) are essential for understanding how a collection of particles move, which is described by the Fokker-Planck equation.

The **Fokker-Planck** equation was first introduced by A. Fokker [**?**] and M. Planck [**?**] in the context of statistical mechanics, and later rederived by A. Kolmogorov [**?**]. It was motivated by the need to describe the transport of an ensemble of particles subject to drag and stochastic forces, in particular the changes in the probability density functions of particles' velocities.

The Fokker-Planck equation can be understood as a phase-space equation that describes (statistically) the spatio-temporal evolution of a collection of particles. It is calculated in the phase space, including, therefore, spatial coordinates ($\vec{r}$), time (t), and momentum variations ($\vec{p}$). If the mass is constant, the variation of the momentum vector translates into the variation of the velocity vector ($\vec{v}$). Given the symmetry of the problem, these vectors wobble around the guiding centre with a given pitch angle. Therefore, one can simplify the treatment by replacing the momentum vectors with the pitch angle (ϕ_p) or its cosine ($\mu \equiv \cos \phi_p$).

The equation reads:

$$\frac{\partial f}{\partial t} + \vec{u} \cdot \vec{\nabla} f - Q = \frac{\partial}{\partial \mu} \left(D_{\mu\mu} \frac{\partial f}{\partial \mu} + D_{\mu p} \frac{\partial f}{\partial p} \right) + \frac{1}{p^2} \frac{\partial}{\partial p} \left(D_{\mu p} \frac{\partial f}{\partial \mu} + p^2 D_{pp} \frac{\partial f}{\partial p} \right) , \qquad (62)$$

where $f = f(\vec{r}, p, t, \mu)$, with $\mu \equiv \cos \phi_p$ (see eq. 31), and $Q = Q(\vec{r}, p, t, \mu)$ symbolises source and sink terms. The coefficients D_{ab} are the diffusion coefficients, particular to a magnetic-field model. The last term in the equation is known as **reacceleration** or **momentum diffusion**. The vector $\vec{u} = \vec{u}(\vec{r})$ denotes the advection velocity, which is a combination of the plasma velocity and Alfvén wave scattering.

The Fokker-Planck coefficients D_{ab} describe the relations

$$D_{ab} = \int\limits_0^\infty dt \left\langle \frac{\partial a(t)}{\partial t} \frac{\partial b(t)}{\partial t} \right\rangle , \tag{63}$$

for any generalised coordinates a and b. The integral can be readily identified as Kubo's equation (eq. 61). Here these coordinates can be the usual spatial coordinates (x, y, z) or the pitch angle[5] (μ). Note that in many cases momentum is one of these generalised coordinates, with their corresponding terms being part of the Fokker-Planck equation (eq. 62).

2.6 Particle decays

Particle decays occur when the lifetime of a given fundamental or composite particle is finite. The time dependence of the number (N) of unstable particles at a time interval between t and $t + dt$ is:

$$\frac{dN}{dt} = -\frac{N}{\tau} , \tag{64}$$

wherein τ is the lifetime of the particle in its own rest frame. This equation can be easily solved, yielding

$$N(t) = N(t_0) \exp\left(-\frac{t}{\tau}\right) , \tag{65}$$

assuming that at at time $t_0 < t$ the number of particles was $N(t_0)$.

One particle can have multiple decay channels. The one that actually occurs depends on the branching ratio $(\mathcal{B})$. Some representative cases useful for high-energy astroparticle physics are listed in table 2.6.

2.6.1 Nuclear decays

Nuclear decays are relevant processes for understanding CR propagation. Three types of decays can be identified.

Alpha decays are characterised by the emission of an alpha particle (or a helium-4 nucleus). For a generic nucleus $^A_Z X$ it can be written as

$$^A_Z X \rightarrow ^{A-4}_{Z-2} X + ^4_2 \alpha ,$$

where X symbolises the new nucleus, and $^4_2 \alpha = ^4_2 He$ is an alpha particle. In this case, the daughter nucleus acquires roughly the Lorentz factor from its parent nucleus if the binding energy per nucleon is small compared to the rest energy of the decay products.

---

[5]Formally, the pitch angle is ϕ_p, but for simplicity $\mu \equiv \cos \phi_p$ will also be used to refer to the pitch angle, interchangeably. The meaning can be implied from the context.

Table 1: Table illustrating the main decay channels for some relevant unstable particles.

particle	lifetime [s]	decay products	branching ratio
μ^-	2.2×10^{-6}	$e^- + \bar{\nu}_e + \nu_\mu$	≈ 1
		$e^- + \bar{\nu}_e + \nu_\mu + \gamma$	6.0×10^{-8}
		$e^- + \bar{\nu}_e + \nu_\mu + e^+ + e^-$	3.4×10^{-5}
π^0	8.5×10^{-17}	$\gamma + \gamma$	0.98823
		$\gamma + e^+ + e^-$	0.01174
		$e^+ + e^- + e^+ + e^-$	3.3×10^{-5}
		$e^+ + e^-$	6.5×10^{-8}
π^+	2.6×10^{-8}	$\mu^+ + \nu_\mu$	0.999877
		$e^+ + \nu_e$	0.000123
n	877.7	$p^+ + e^- + \bar{\nu}_e$	≈ 1
		$p^+ + e^- + \bar{\nu}_e + \gamma$	10^{-9}
^3_1H	3.9×10^8	$^3_2\text{He} + e^- + \bar{\nu}_e$	≈ 1

Beta decays consist in the conversion of a neutron into a proton (β^+ decay):

$$^A_Z\text{X} \to ^A_{Z+1}\text{X} + e^- + \bar{\nu}_e \,,$$

or in the conversion of a proton into a neutron (β^- decay):

$$^A_Z\text{X} \to ^A_{Z-1}\text{X} + e^+ + \nu_e \,.$$

Note that this is an important channel for neutrino production by nuclei.

In **gamma decays** a photon is *spontaneously* emitted by an unstable nucleus:

$$^A_Z\text{X} \to ^A_Z\text{X} + \gamma \,.$$

The combination of the number of protons (Z) and of the number of neutrons ($N = A - Z$) can, in principle, be completely arbitrary, regardless of whether it results in a stable nucleus or not. However, for some combinations of Z and N, this would inevitably result in immediate decays via **nucleon dripping**, which consists in the mission of a proton or a neutron of same isospin. As in the case of alpha decay, at high energies the leaked nucleons approximately retain the parent's Lorentz factor. The number of decay channels for various combinations of Z and N are shown in the left panel of figure 5. The main decay modes for each nucleus are shown in the right panel.

Nuclear lifetimes are measured in laboratory and compiled in databases such as NuDat database[6] [**? ?**], which also allows interactive search of decay radiation and nuclear structural information.

2.7 Photonuclear interactions

Photonuclear interactions involve the interaction of a nucleus X, with atomic mass A, composed of Z protons (^A_ZX). They are generally written as $^A_Z\text{X} + \gamma_{\text{bg}} \to \dots$. The exact interaction taking place depends on the cross section for the processes, which is a consequence of the spectral energy distribution of background photons (γ_{bg}) and on the energy of the nucleus. The ellipsis ('...') indicate the results of the interaction, which depends on the spectral distribution of background
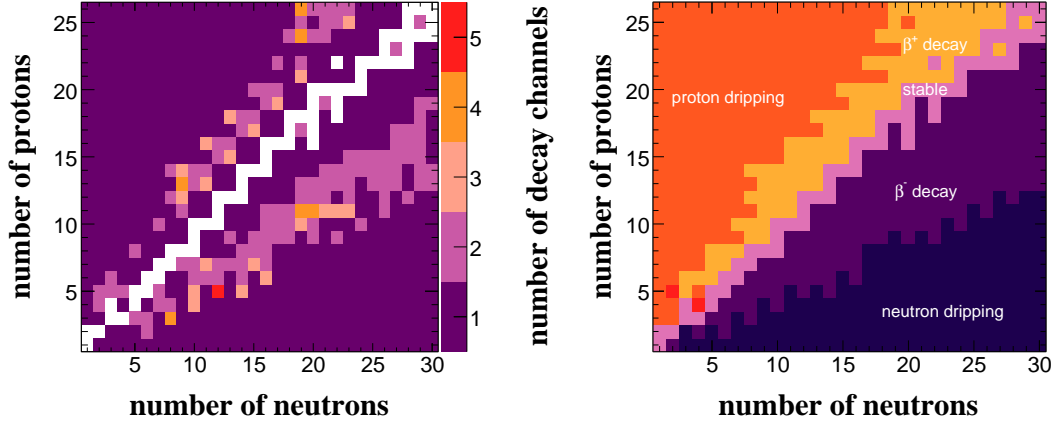
---

[6]https://www.nndc.bnl.gov/nudat3/

Figure 5: The number of decay channels for each combination of proton (Z) and neutron (N) number are shown in the left panel. The white regions correspond to stable nuclei, with no (known) decay modes. The dominant decay channels for these nuclei are shown in the right panel. Figure taken from ref. [?].

photons as well as on the energy of the nucleus. Some of the processes relevant for high-energy modelling are listed below.

2.7.1 Bethe-Heitler pair production

When a nucleus interacts with a background photon (γ_{bg}) electron-positron pairs can be created [?]. This is described by the reaction: $^A_Z X + \gamma_{bg} \rightarrow ^A_Z X + e^+ + e^-$. It is essentially the equivalent to bremsstrahlung radiation with a photon instead of an electron/positron on the left side of the reaction.

Let E be the energy of a nucleus of atomic number Z and mass A. The energy loss by a nucleus $^A_Z X$ per unit distance is the same rate at which electrons (and positrons) gain energy if the energy of the background photon is much smaller than the rest mass of electrons. It reads

$$\frac{dE}{dx} = -\alpha r_0^2 Z^2 (m_e c^2)^2 \int\limits_2^\infty d\xi\, n\left(\frac{\xi m_e c^2}{2\gamma}\right) \frac{\phi(\xi)}{\xi^2}, \tag{66}$$

where r_0 is the classical radius of the electron, α is the fine-structure constant, $\xi \equiv 2\gamma\varepsilon/(m_e c^2)$, and $\phi(\xi)$ is a function of the differential cross sections (for details see ref. [?]).

In the particular case of a blackbody of temperature T, as is the CMB, eq. 66 reduces to [?]:

$$\frac{dE}{dx} = -\frac{\alpha r_0^2 Z^2 (m_e c^2 k_B T)^2}{\pi^2 \hbar^3 c^3} \left(\frac{m_e c^2}{2\gamma k_B T}\right)^2 \int\limits_2^\infty d\xi\, \frac{\phi(\xi)}{\exp\left(\frac{m_e c^2}{2\gamma k_B T}\xi\right) - 1}. \tag{67}$$

Bethe-Heitler pair production takes place if the energy of the background photon in the nucleus rest frame is $\varepsilon' \gtrsim 1$ MeV. Alternatively, in the laboratory frame, the threshold condition becomes

$$E \gtrsim 5 \times 10^{20} A \left(\frac{\varepsilon}{\text{eV}}\right) \text{ eV}.$$

Note that the treatment above ignore possible screening effects, which are expected to be small

at high energies [**?**]. Moreover, it neglects possible polarisation effects that could arise, which are unimportant in the ultrarelativistic regime [**? ?**].

For UHECRs traversing cosmic expanses, the mean free path for Bethe-Heitler pair production is fairly small, but so is the inelasticity of the process ($\lesssim 10^{-3}$). This has implications for the choice of algorithm to treat this problem computationally, as discussed in §3.3 and §4.7.2.

Remarkably, it has been postulated that this process underlies the origin of the *ankle* feature in the cosmic-ray spectrum if UHECRs consist exclusively of protons [**?**]. Yet, for atomic nuclei, the energy loss scales are roughly proportional to Z^2/A in comparison to proton energy losses.

Comprehensive investigations concerning the differential energy loss rate arising from this mechanism, as well as the resultant spectrum of generated electron-positron pairs, have been detailed in refs. [**? ?**].

2.7.2 Photomeson production

The generation of mesons resulting from the interaction between a cosmic-ray nucleus ($_Z^A$X) and a background photon (γ_{bg}) holds immense significance within the multimessenger framework, as it yields both neutrinos and photons. For instance, when considering protons, in their rest frame, the interaction with photons with energies $\varepsilon' \gtrsim 1$ GeV is characterised by the dominance of a short-lived resonance. This resonance rapidly transforms into mesons and other secondary particles. As energy levels escalate, the potential for multiple particle generation during a single interaction also increases. Furthermore, direct meson production is feasible at these elevated energies.

An important process in photonuclear meson interactions is the production of pions. For UHE protons, this process triggers a Δ^+ resonance, which subsequently decays into either protons and neutral pions ($_Z^A$X $+ \gamma_{bg} \to \Delta^+ \to p + \pi^0 + \ldots$) or neutrons and charged pions ($_Z^A$X $+ \gamma_{bg} \to \Delta^+ \to n + \pi^+ + \ldots$). The decay of the pions (see §2.6) generate copious amounts of photons and neutrinos. Notably, this mechanism gives rise to the Greisen–Zatsepin–Kuzmin (GZK) cutoff, stemming from UHE protons interacting with the CMB [**? ?**].

The cross section for the interaction of a nucleon (proton or neutron) with a background photon in the rest frame of the nucleon is shown in figure 6.

However, addressing these interactions for atomic nuclei is more complicated due to screening effects[7]. Unlike in the proton case, the target photon does not interact uniformly with all nucleons constituting the nucleus. Instead, a scaling relation based on the numbers of protons and neutrons is often employed to derive the mean free path (as seen in references like [**?**]). This approach can be problematic, as it has been demonstrated to deviate from measured cross sections, significantly impacting predictions of secondary neutrino and photon fluxes [**?**].

2.7.3 Photodisintegration

Interactions involving cosmic rays and background photons can fragment nuclei into smaller constituents: $_Z^A$X $+ \gamma_{bg} \to_{Z'}^{A'}$ X $+ \ldots$. This phenomenon is usually interpreted as two sequential sub-processes, the first being photoabsorption by the nucleus, which creates an excited state, and its subsequential decay that often emits nucleons [**?**].

---

[7]Screening effects can be understood by envisioning a nucleus gathering A protons and neutrons in total. The three-dimensional arrangement of these nucleons will create layers, some of which will be "hidden" in the inner-most parts of the nucleus and not directly exposed. It follows from this simple intuitive reasoning that only a fraction of the nucleons will be on the surface and act as targets for interactions. A first guess would be that this relates to the ratio between surface area and volume, for a collection of A nucleons, revealing about $A^{2/3}$ of them.
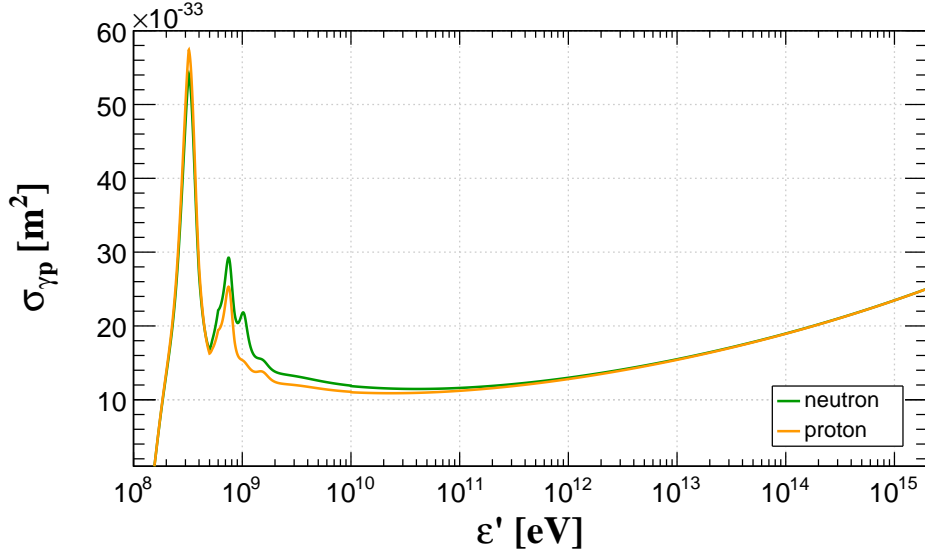
Figure 6: The graph shows the total cross section for $p + \gamma_{\text{bg}} \rightarrow$ meson and $n + \gamma_{\text{bg}} \rightarrow$ meson, as a function of the background photon energy in the nucleon rest frame (ε'). Figure taken from ref. [**?**].

Photodisintegration of very energetic cosmic-ray nuclei has been studied in the past by several authors [**? ? ?**], but only in recent years has it evolved to reduce uncertanties [**? ? ?**]. Nevertheless, these cross section still remains a prominent source of uncertainty in UHECR propagation [**?**].

The outcomes of photodisintegration are exemplified by processes such as:

- proton emission: $^{A}_{Z}\text{X} + \gamma_{\text{bg}} \rightarrow^{A-1}_{Z-1} \text{X} + p$;
- neutron emission: $^{A}_{Z}\text{X} + \gamma_{\text{bg}} \rightarrow^{A-1}_{Z} \text{X} + n$;
- α-particle emission: $^{A}_{Z}\text{X} + \gamma_{\text{bg}} \rightarrow^{A-4}_{Z-2} \text{X} +^{4}_{2} \text{He}$.

In the UHE domains, the photodisintegration cross section is significantly influenced by two components. The first is the giant dipole resonance (GDR), which dominates at photon energies $\varepsilon' \lesssim 50\,$MeV in the nucleus rest frame. The other is the quasi-deuteron (QD) emission, prevalent in the energy range $50 \lesssim \varepsilon'/\text{MeV} \lesssim 150$.

When modelling photodisintegration processes, it is important to bear in mind that photonuclear cross sections are not fully known. As a consequence, they can have a considerable impact in the propagation of UHECRs [**? ? ?**]. Consequently, this knowledge gap holds the potential to substantially impact the consequent production of photons and neutrinos [**?**].

2.7.4 Photonuclear elastic scattering

Nuclei can undergo interactions with background photons and simply transfer energy to them. This process is known as elastic scattering: $^{A}_{Z}\text{X} + \gamma_{\text{bg}} \rightarrow^{A}_{Z} \text{X} + \gamma$. At ultra-high energies, this is subdominant compared to photodisintegration.

Elastic scattering is negligible as an energy-loss mechanism of nuclei, but it can be important in computing photon fluxes produced by energetic cosmic-ray nuclei.

2.8 Hadronuclear interactions

Hadronuclear interactions are generally elaborate and cannot be exactly described. This is because the underlying theory of strong interactions, quantum chromodynamics (QCD), poses major challenges in terms of computational treatment.

2.8.1 Proton-proton interactions

For proton-proton interaction, there are several possible channels. The overwhelming majority result in the production of pions. Some of these channels are shown below.

$$p + p \rightarrow p + p + \pi^0 \,,$$
$$p + p \rightarrow p + p + \pi^0 + \pi^0 \,,$$
$$p + p \rightarrow p + n + \pi^+ + \pi^0 \,,$$
$$p + p \rightarrow p + n + \pi^+ + \pi^- + \pi^0 \,.$$

The cross section for proton-proton interactions is not exactly known. Instead, it is obtained through a combination of measurements [? ? ? ? ? ? ?] and extrapolation to higher energies using hadronic interaction models [? ? ? ?]. One possible parametrisation was provided in ref. [?]:

$$\sigma_{\text{ine}}^{pp}(x) = \left[30.7 - 0.96 \log(x) + 0.18 \log^2(x)\right] \left[1 - x^{-1.9}\right] \, 10^{-31} \, \text{m}^2 \,, \tag{68}$$

where

$$x(E) = \frac{E - m_p c^2}{2 m_{\pi^0} c^2 + \frac{m_{\pi^0}^2 c^2}{2 m_p}} \,, \tag{69}$$

with m_p denoting the mass of a proton with energy E (measured in the lab frame), and m_{π^0} representing the mass of the neutral pion.

It is worth stressing that many theoretical uncertainties remain in the measurement of the proton-proton cross section, despite the increasingly more accurate data being delivered. In particular, the relative contribution of the elastic with respect to the inelastic cross sections is far from clear, as is the differential cross sections and the scattering amplitudes. For more details see, e.g., refs. [? ? ?].

2.8.2 Nucleus-nucleus interactions

For nucleus-nucleus interactions, Glauber theory [?] can be employed. In this case, the collision can be modelled as a succession of scattering between a nucleon from one of the nuclei, and a nucleon from the other. Even though this is an approximation, it sets an upper limit to the total inelastic cross section, which should be smaller than the sum of all individual nucleon-nucleon cross sections. This approximation is not adequate for lighter nuclei [?].

The nucleus-nucleus cross section can be approximated as [?]

$$\sigma_{\text{ine}}^{A_i, A_t}(x) = \pi r_0^2 \left[A_i^{1/3} + A_t^{1/3} - b_0 \left(A_i^{-1/3} + A_t^{-1/3}\right)\right] \max\left\{1, \log\left(\frac{\sigma_{\text{ine}}^{pp}(x)}{\sigma_{\text{ine}}^{pp}(x_0)}\right)\right\} \,, \tag{70}$$

wherein A_i and A_t refer to the atomic mass of the incident and target nuclei, respectively, and the

coefficient b_0, empirically obtained, reads [?]

$$b_0 = \begin{cases} 2.247 - 0.915 \left(1 + A_t^{-1/3}\right) & \text{if } i = {}^1\text{H}, \\ 1.581 - 0.876 \left(A_i^{-1/3} + A_t^{-1/3}\right) & \text{if } i \neq {}^1\text{H}. \end{cases} \tag{71}$$

The variable χ is conveniently defined in terms of the kinetic energy per nucleon of the incident particle

$$\chi(E) = \frac{E - m_{A_i} c^2}{A \left(2 m_{\pi^0} c^2 + \frac{m_{\pi^0}^2 c^2}{2 m_p}\right)}, \tag{72}$$

where σ_{ine}^{pp} as in eq. 68 and $\chi_0 \equiv x(1 \text{ PeV})$.

Nucleus-nucleus interactions are usually treated by employing event generators, which are libraries that models a given particle interaction based on their initial state, accounting for the stochasticity of the process at hand. Some widely used event generators include PYTHIA[8] [? ?], HERWIG [? ? ?], and Sherpa [?], among others. For higher energy studies, in particular the interaction of CRs with air, commonly used hadronic interaction codes are EPOS [?], QGSJet [? ? ?], and Sibyll [? ?]. Note, however, that at UHEs, these generators are limited by the availability (or actually lack thereof) of accelerator data, since they operate at much higher energies than what current accelerators can reach.

For astrophysical applications, hadronuclear interactions are usually parametrised based on simulations. Common parametrisations includes those from refs. [? ? ?]. One can argue that considering all other astrophysical uncertainties, the parametrisations provide an adequate approximation. However, recent simulation-based studies challenge this assertion [?].

2.9 Electromagnetic interactions

2.9.1 Pair production

Breit-Wheeler pair production is one of the simplest processes in quantum electrodynamics (QED). It is essentially the direct production of an electron-positron pair due to the interaction of two photons: $\gamma + \gamma_{\text{bg}} \to e^+ + e^-$ [?]. The cross section for this process is well-known:

$$\sigma(\beta) = \frac{3\sigma_{\text{T}}}{16} \left(1 - \beta^2\right) \left[\left(3 - \beta^4\right) \ln\left(\frac{1+\beta}{1-\beta}\right) - 2\beta \left(2 - \beta^2\right)\right], \tag{73}$$

where σ_{T} represents the Thomson cross section, and

$$\beta = \sqrt{1 - \frac{4 m_e^2 c^4}{s}}. \tag{74}$$

Here s is the squared centre of mass energy, which for a high-energy photon with energy E scattering off a low-energy background photon of energy ε reads

$$s = 2E\varepsilon \left(1 - \cos\theta\right), \tag{75}$$

---

[8]See ref. [?] for a historical overview of this widely-used event generator.

wherein θ denotes the collision angle. It follows immediately that the kinematic thresholds for this interaction are $s_{\min} = m_e^2 c^4$ and $s_{\max} = m_e^2 c^4 + 2E\varepsilon_{\max}(1+\beta)$.

It is natural to think that electrons and positrons will have approximately the same energy. In the high-energy regime ($s \gg m_e^2 c^4$), also known as the Klein-Nishina limit, this is not necessarily true. In this case, the energy of the leptons produced will depend on the differential cross section for the process:

$$\frac{d\sigma}{dy} \propto \frac{1}{y}\left[\frac{y^2}{1-y} + 1 - y + \frac{(1-\beta^2)^2}{4y(1-y)^2}\right]\frac{1}{1+2\beta^2 - 2\beta^4}, \tag{76}$$

where y is the fraction of the energy of the energetic photon being taken by one of the particles produced. The other particle, evidently, takes a fraction of the primary's energy of $1 - y$.

2.9.2 Inverse Compton scattering

This basic quantum electrodynamics (QED) process is described by the reaction: $e^\pm + \gamma_{bg} \to e^\pm + \gamma$. Inverse Compton scattering (ICS) is, therefore, a simple momentum exchange, as is the usual Compton effect [?], but in this case involving a high-energy electron and low-energy photons instead of the opposite. *Compton effect*, both the direct and the inverse, constitute one of the most important milestones of 20th-century physics [?] with far-reaching consequences in several sub-fields of physics, especially astrophysics.

The squared centre-of-mass energy (s) is

$$s = m_e^2 c^4 + 2E\varepsilon\left(1 - \beta\cos\theta\right), \tag{77}$$

with β given by

$$\beta = \frac{s - m_e^2 c^4}{s + m_e^2 c^4}. \tag{78}$$

Its kinematic threshold is simply the requirement that the electron continues to exist after the collision: $s_{\min} = m_e^2 c^4$.

The cross section for ICS can be written as [?]

$$\sigma(s) = \frac{3\sigma_T}{8\beta}\frac{m_e^2 c^4}{s}\left[\frac{2}{\beta(1+\beta)}(2 + 2\beta - \beta^2 - 2\beta^3) - \frac{1}{\beta^2}(2 - 3\beta^2 - \beta^3)\ln\left(\frac{1+\beta}{1-\beta}\right)\right]. \tag{79}$$

In the low-energy limit ($s \sim m_e^2 c^4$), eq. 79 reduces to the usual Thomson scattering result ($\sigma \approx \sigma_T$).

After the scattering the electron (or positron), which had an initial energy E, will have energy E', as dictated by the differential cross section [?]:

$$\frac{d\sigma}{dE'} = \frac{3\sigma_T}{8E}\frac{m_e^2 c^4}{s}\frac{1+\beta}{\beta}\left[y + \frac{1}{y} + \frac{2(1-\beta)}{\beta}\left(1 - \frac{1}{y}\right) + \frac{(1-\beta)^2}{\beta^2}\left(1 - \frac{1}{y}\right)^2\right], \tag{80}$$

with $y \equiv E'/E$.

2.9.3 Double pair production

Double pair production is the higher-order counterpart of the usual pair production. It can be written as $\gamma + \gamma_{bg} \to e^+ + e^- + e^+ + e^-$. Its possible role in energetic astrophysical processes has long been investigates [? ?].

The centre-of-mass energy for this process is the same as that for pair production (eq. 75):

$$s = 2E\varepsilon \left(1 - \cos\theta\right) . \tag{81}$$

This interaction has a final state composed of four electrons, so the threshold is $s_{\mathrm{min}} = 16 m_e^2 c^4$.

The high-energy limit of its cross section $(s \gg 16 m_e^2 c^4)$ is [?]:

$$\sigma(s) = \sigma_\infty \left[1 - \frac{16 m_e^2 c^4}{s}\right]^6 , \tag{82}$$

where $\sigma_\infty = 6.45 \times 10^{-34}$ m^2.

The energy distribution of the electrons and positrons generated are more difficult to be obtained. For one of them, a differential cross section of the form

$$\frac{\mathrm{d}\sigma}{\mathrm{d}E_\star'} = \frac{1}{\sqrt{s}} g\left(\frac{2E_\star'}{\sqrt{s}}, s\right) \sigma_{\mathrm{tot}}(s) \tag{83}$$

can be written, wherein the quantities marked with a '$\star$' are measured in the centre of mass frame, such that $E_\star'$ is the energy of one of the produced particles in this frame. The function g cannot be obtained in a straightforward manner. According to ref. [?], a reasonable assumption is that at such high energies one of the pairs receive all the energy, and each of its components takes half of the energy, which implies

$$g\left(\frac{2E_\star'}{\sqrt{s}}\right) = 2\delta\left(\frac{2E_\star'}{\sqrt{s}} - \frac{1}{2}\right) , \tag{84}$$

with δ referring to the Dirac delta function. A more detailed calculation employing event generators was conducted by the authors of ref. [?], who provided a fit to the results:

$$g\left(\frac{2E_\star'}{\sqrt{s}}\right) = \frac{5}{3} + \left(\frac{4E_\star'}{\sqrt{s}} - 1\right)^2 . \tag{85}$$

2.9.4 Triplet production

Triplet pair production is related to inverse Compton scattering, but instead of a photon at the end of the process a pair is created: $e^\pm + \gamma_{\mathrm{bg}} \to e^\pm + e^+ + e^-$. Its role in the propagation of particles has been identified long ago [? ?].

Being closely related to inverse Compton scattering, the squared centre-of-mass energy for this process is the same:

$$s = m_e^2 c^4 + 2E\varepsilon \left(1 - \beta \cos\theta\right) . \tag{86}$$

The final state contains three electrons, such that this process occurs only above the threshold $s_{\mathrm{min}} = 9 m_e^2 c^4$.

Its cross section in the high-energy limit $(s \gg m_e^2 c^4)$ is [?]

$$\sigma(s) = \frac{3\alpha\sigma_{\mathrm{T}}}{8\pi} \left[\frac{28}{9} \ln\left(\frac{s}{m_e^2 c^4}\right) - \frac{218}{27}\right] . \tag{87}$$

In this regime the differential cross section for one particle of the produced pair with energy E' can be written simply as a power law:

$$\frac{\mathrm{d}\sigma}{\mathrm{d}E'} \propto E'^{-7/4} . \tag{88}$$

27

2.10 Particle mixing

Processes other than interactions and decays that change the nature of a particle also exist. Within a quantum-mechanical framework, they are usually described by a mixing of some intrinsic eigenstates[9] of a family of particles ($\mathfrak{X}$), which results in propagation eigenstates[10] (X). This notion can be mathematically expressed as

$$
\begin{pmatrix} X_1 \\ \vdots \\ X_n \end{pmatrix} = \begin{pmatrix} U_{11} & \dots & U_{1n} \\ \vdots & \ddots & \vdots \\ U_{n1} & \dots & U_{nn} \end{pmatrix} \begin{pmatrix} \mathfrak{X}_1 \\ \vdots \\ \mathfrak{X}_n \end{pmatrix} , \tag{89}
$$

where X_i refers to the particle being observed. Here U_{ij} are elements of U, the **mixing matrix**.

If U is diagonal, then there is no *mixing* between states. In this case, the intrinsic states of the particles are exactly equal to the propagation eigenstates. However, if there are non-vanishing off-diagonal elements, the corresponding states will mix among themselves.

The intrinsic eigenstates, by definition, are the free (i.e., in the absence of any potentials) particle solutions to the wave equation, and thus can be written as

$$
|X_i(t)\rangle = |X_i\rangle \exp\left[i\left(\vec{p}_i \cdot \vec{r} - E_i t\right)\right] , \tag{90}
$$

where $\vec{p}_i$ and E_i denote the momentum and energy of particle X_i, respectively.

The mixing of states is described by the Schrödinger equation:

$$
i\frac{\mathrm{d}|\psi\rangle}{\mathrm{d}t} = H|\psi\rangle , \tag{91}
$$

wherein H is the Hamiltonian of the system and

$$
|\psi\rangle = \sum_{j=1}^{n} c_j |X_j\rangle , \tag{92}
$$

for arbitrary constants c_j satistfying the condition $\sum_j |c_j|^2 = 1$.

The time-evolution operator, assuming that the H is time-independent, is defined as

$$
U(t) = \exp\left(-iHt\right) . \tag{93}
$$

The connection between intrinsic and propagation eigenstates through the unitary ($U^\dagger U = \mathbb{I}$) matrix U is

$$
|X_i\rangle = \sum_{j=1}^{n} U_{ij} |\mathfrak{X}_j\rangle . \tag{94}
$$

---

[9]This terminology is not found elsewhere in the literature. In principle, there is no such thing as an *intrinsic eigenstate*, since any basis can be chosen to describe the same phenomenon. Depending on one's philosophical inclinations, what I am calling intrinsic eigenstates can have an *ontological* meaning, with direct correspondence with real-world entities. However, for the purposes of this discussion it suffices to understand these states as the eigenstates of the free Hamiltonian.

[10]Once again, I make up a nomenclature that is not usually found in the literature, *propagation eigenstate*. This refers to the states represented in a basis convenient for describing what is actually observed after the particle, which is a quantum superposition of states, travelled a certain distance.

Conversely, since U is unitary,

$$|\mathfrak{X}_i\rangle = \sum_{j=1}^{n} U_{ij}^* |X_j\rangle . \tag{95}$$

The probability (P_{X_i}) that a state X_i will be detected after the particle travelled a distance L is simply the sum of the probabilities of each component ending up as X_i:

$$P_{X_i}(L) = \sum_{j=1}^{n} \left| \langle X_i | \mathfrak{X}_j \rangle \right|^2 . \tag{96}$$

The general form given by eq. 89 can be applied to many problems, the most notorius of which is neutrino oscillations, described in §2.10.1

2.10.1 Neutrino oscillations

Neutrinos are detected in what is called *flavour states* — the electron (ν_e), the muon (ν_μ) and the ν_τ neutrinos — the **flavour eigenstates**, which correspond to what had been previously been called propagation eigenstates. However, they are a superposition of intrinsic eigenstates, which for neutrinos are *mass eigenstates*[11].

The original idea of neutrino oscillations dates back to the late 1950s, building on the work of B. Pontecorvo [?]. The underlying theory of oscillations was further developed in the following decade by others [? ?]. Only towards the end of the 20th century has this phenomenon been unambiguously confirmed through observations of solar neutrinos [? ?].

Let ν represent the flavour state of a neutrino, and υ its mass state. If propagation is in vacuum, the mixing matrix (U) has the general form

$$U = \begin{pmatrix} U_{e1} & U_{e2} & U_{e3} \\ U_{\mu1} & U_{\mu2} & U_{\mu3} \\ U_{e\tau1} & U_{\tau2} & U_{\tau3} \end{pmatrix} , \tag{97}$$

where U_{e1} refers to the mixing between the mass eigenstate 1 and the flavour state corresponding to the electron neutrino (e), and similarly for the other terms. U is the so-called Pontecorvo-Maki-Nakagawa-Sakata (PMNS) matrix, given by

$$U = \begin{pmatrix} c_{12}c_{13} & s_{12}c_{13} & s_{13}e^{-i\delta} \\ -s_{12}c_{23} - c_{12}s_{23}s_{13}e^{i\delta} & c_{12}c_{23} - s_{12}s_{23}s_{13}e^{i\delta} & s_{23}c_{13} \\ s_{12}s_{23} - c12c_{23}s_{13}e^{i\delta} & -c_{12}s_{23} - s12c_{23}s_{13}e^{i\delta} & c_{23}c_{13} \end{pmatrix} \begin{pmatrix} e^{i\alpha_1/2} & 0 & 0 \\ 0 & e^{i\alpha_2/2} & 0 \\ 0 & 0 & 1 \end{pmatrix} , \tag{98}$$

wherein $c_{ij} \equiv \cos\theta_{ij}$ and $s_{ij} \equiv \sin\theta_{ij}$, and α_i in the right-most matrix is related to whether neutrinos are Dirac or Majorana particles.

Eq. 98, together with eq. 96, allow the calculation of oscillation probabilities, which is used to infer neutrino states after propagating in the universe. Note, however, that this assumes propagation in vacuum. While this assumption is adequate for many applications, this is not always the case. For

---

[11]Sometimes the mass eigenstates are referred to as *physical eigenstates*. I prefer to avoid such terminology, due to the philosophical implications of the word 'physical'. There is no guarantee that the mass eigenstates have direct correspondence to what really exists in reality. In fact, what we call neutrinos might simply be a manifestation of other yet-unknown phenomenon which, in this view, would be even more "physical".

that the Hamiltonian that goes into the Schrödinger equation (eq. 91) would change, making the treatment more complicated and often requiring advanced computational methods for the solution.

2.11 Other energy loss processes

2.11.1 Synchrotron cooling

When exposed to a magnetic field, charged particles can release synchrotron radiation. For a particle of mass m and charge q, moving with momentum $\vec{p}$, the energy loss per unit length is given by:

$$\frac{\mathrm{d}E}{\mathrm{d}x} = -\frac{q^4}{6\pi\epsilon_0 c^4 m^4}\left|\vec{p}\times\vec{B}\right|, \tag{99}$$

where ϵ_0 denotes the vacuum permittivity, and $\vec{B}$ represents the magnetic field. It is important to note that when the particle's motion aligns with the magnetic field, i.e., $\vec{p}\parallel\vec{B}$, no radiation is emitted.

The radiated synchrotron spectrum is strongly peaked around the critical energy,

$$E_{\mathrm{c}} = \frac{3}{2}\hbar c\gamma^3 q\frac{1}{p^2}|\vec{B}\times\vec{p}|. \tag{100}$$

It can be decomposed as a sum of two components, a parallel ($I_{\parallel}$) and a perpendicular ($I_{\perp}$) one, given by [?]

$$\frac{\mathrm{d}I_{\perp}}{\mathrm{d}y} \propto F(y) + G(y), \tag{101}$$

$$\frac{\mathrm{d}I_{\parallel}}{\mathrm{d}y} \propto F(y) - G(y). \tag{102}$$

$$\tag{103}$$

Here the auxiliary functions $F(y)$ and $G(y)$ are [?]

$$F(y) = y\int_y^\infty K_{\frac{5}{3}}(y')\mathrm{d}y' \tag{104}$$

and

$$G(y) = yK_{\frac{2}{3}}(y), \tag{105}$$

where $K_{\frac{5}{3}}$ is a modified Bessel function and $y \equiv E_\gamma/E_{\mathrm{c}}$.

While the impact of synchrotron emission remains negligible for atomic nuclei journeying across cosmic distances, largely due to the relatively low strengths of IGMFs [? ? ?], it becomes important in the environment of astrophysical sources, especially those with stronger magnetic fields. In these environments, synchrotron radiation can potentially lead to distinctive spectral signatures that allow for the deduction of magnetic field characteristics in these regions [? ?].

2.11.2 Adiabatic cosmological losses

Energy losses occur for all particles, due to the adiabatic expansion of the Universe. The change in redshift ($\mathrm{d}z$) corresponding to an infinitesimally small distance $\mathrm{d}\ell$ is described by the equation:

$$dz = \frac{H_0}{c}\sqrt{\Omega_\Lambda + \Omega_m(1+z)^3}\, d\ell\,. \tag{106}$$

Here, H_0 is the current Hubble parameter, approximately $67.3\ \text{km}\,\text{s}^{-1}\,\text{Mpc}^{-1}$, and Ω_m and Ω_Λ stand at about 0.3147 and 0.6853 respectively, representing the matter and dark-energy densities within the flat Λ cold dark matter (ΛCDM) model, as per references [?]. It is worth noting that eq. 106 would include an additional term accounting for radiation, although it is only relevant during the very early stages of the universe's life ($z \gtrsim 1000$).

3   Building propagation models

3.1   Prescriptions for generating turbulent magnetic fields

The generation of turbulent stochastic magnetic fields, as described in 2.5.1, requires somewhat advanced computational methods. Here I will present a sampling strategy relying on the Fourier spectrum of the field, taking advantage of the equations from §2.5.1 [? ? ?].

I will present a general strategy for sampling a field with spectral index α_B (see eq. 24) limited to a range in Fourier space $k_{min} < k < k_{max}$. Because this approach relies on the expansion of the magnetic field into a base containing two circularly polarised modes ($\{\hat{e}_+, \hat{e}_-\}$), this strategy is also suitable for simulating helical magnetic fields.

I will refrain from providing the full derivation; for the whole derivation the reader is referred to ref. [?]. I will start with eq. 25 of this reference, transcribed below:

$$\tilde{\vec{B}}(\vec{k}) = \tilde{B}_+(\vec{k})\hat{e}_+(\vec{k}) + \tilde{B}_-(\vec{k})\hat{e}_-(\vec{k})\,, \tag{107}$$

with the tilde indicating that the quantity is in Fourier space. In this case, the usual basis $\{\hat{x}, \hat{y}, \hat{z}\}$ (in Fourier space) can be recast onto $\{\hat{e}_1, \hat{e}_2, \hat{e}_3\} \equiv \{\hat{e}_+, \hat{e}_-, \hat{k}\}$. Furthermore, $\tilde{B}_\pm$ is

$$\tilde{B}_\pm(\vec{k}) \equiv |\tilde{\vec{B}}_\pm(\vec{k})| = |\tilde{B}_\pm(\vec{k})|\left[\cos\theta_\pm(\vec{k}) + i\sin\theta_\pm(\vec{k})\right]\,, \tag{108}$$

wherein $0 \leq \theta_\pm(\vec{k}) < 2\pi$ are random phases uniformly distributed in the interval. The generation of a turbulent magnetic field distribution, therefore, can be done by sampling $\theta_\pm$ from a uniform distribution. The norm, $\tilde{B}_\pm$, is generated from a zero-mean Gaussian with standard deviation given by the desired RMS of the field (see eq. 18). Note that this procedure is done for a grid with (N_x, N_y, N_z) cells.

Once $\tilde{\vec{B}}(\vec{k})$ is sampled using the procedure described above, a Fourier transform can be applied to bring this quantity to real space:

$$\vec{B}(\vec{r}) = \mathfrak{Re}\left(\mathcal{F}\left\{\tilde{\vec{B}}_\pm(\vec{k})\right\}\right)\,. \tag{109}$$

Here $\mathcal{F}$ is the Fourier transform operator, and $\mathfrak{Re}$ is a function that takes the real part of the argument. This result is subsequently normalised to the desired field RMS (labelled B_{rms}), such that $\vec{B}(\vec{r})$ is recast as

$$\vec{B}(\vec{r}) = B_{rms}\left[\frac{1}{N_x N_y N_z}\sum_{i=1}^{N_x}\sum_{j=1}^{N_y}\sum_{k=1}^{N_z}\vec{B}(\vec{r}_{ijk})\cdot\vec{B}(\vec{r}_{ijk})\right]^{-\frac{1}{2}}\vec{B}(\vec{r})\,, \tag{110}$$

where $\vec{r}_{ijk}$ refers to the position vector in each cell of this grid.

Note that the non-helical case can be obtained by taking $\theta_{\pm}$ different for the two components of this basis, $\hat{e}_+$ and $\hat{e}_-$. This effectively averages over the two polarisation modes that would not exist if helicity had been neglected.

3.2 Particle trajectories in the presence of magnetic fields

Charged particles like cosmic-ray nuclei and electrons can be deflected in the presence of magnetic fields. The equations of motion were already presented in §2.5.

In this section a few strategies to implement algorithms to solve them are presented. Single-particle propagation algorithms are presented in §3.2.1 and §3.2.2. Methods for modelling the transport of an ensemble of particles are described in §3.2.3.

3.2.1 Runge-Kutta algorithm

Runger-Kutta (RK) methods are numerical solvers for differential equations [? ?]. They solve all equations simultaneously at discrete steps.

A set of six differential equations (eqs. 27 and 28) can be solved a N-th order RK method, where the order of the solver is typically $N = 4$ (RK4) or $N = 5$ (RK5). These equations take the general form

$$\frac{\mathrm{d}y}{\mathrm{d}t} = f(t, x), \tag{111}$$

with initial condition $y(t_0) = y_0$. Here y are placeholders for the phase space components, the position ($\vec{r}$) and momentum ($\vec{p}$).

First, space has to be discretised into steps. The initial conditions are known, and so are the properties of a particle at the first step. The subsequent propagation steps are obtained based on the previous ones.

In **explicit RK methods** the equations are solved at each step, as follows:

$$y_{n+1} = y_n + s \sum_{i=1}^{n_s} b_i k_i, \tag{112}$$

where n indicates the step at which the calculation is being performed, s is the step size, b_i is a coefficient, and n_s relates to the order of the RK method. The values of k_i are:

$$k_1 = f(t_n, y_n), \tag{113}$$
$$k_2 = f\left(t_n + c_2 s, y_n + s\left(a_{21} k_1\right)\right), \tag{114}$$
$$k_3 = f\left(t_n + c_3 s, y_n + s\left(a_{31} k_1 + a_{32} k_2\right)\right), \tag{115}$$
$$\cdots \tag{116}$$
$$k_i = f\left(t_n + c_i s, y_n + s \sum_{j=1}^{n_s} a_{ij} k_j\right). \tag{117}$$

The coefficients c_i can be obtained from the numerical tables.

Adaptative RK methods are a class of implicit algorithms that extended the previous idea. They automatically allow for suitable choices of step sizes to keep the errors below a certain tolerance. In

this case, the steps are:

$$y_{n+1}^{\star} = y_n + s \sum_{i=1}^{n_s} b_i^{\star} k_i \,. \tag{118}$$

The condition to adjust the step size requires the calculation of the associated error, which is

$$\epsilon_{n+1} = y_{n+1} - y_{n+1}^{\star} = s \sum_{i=1}^{n_s} b_i k_i - b_i^{\star} k_i \,. \tag{119}$$

The coefficients can be taken from look-up tables. A commonly used one constitutes the Cash-Karp (CK) [?], with a wide array of applications in astrophysics.

3.2.2   Boris push algorithm

The Boris push (BP) algorithm [?] is the state of the art for solving the equation of motion of a charged particle in a magnetised medium. Unlike the RK method which solves a system of couple differential equations, the BP algorithm solves the equations of motion related to the Lorentz force. It is highly accurate without sacrificing efficiency [?], outperforming the usual adaptative RK method with CK coefficients by up to an order of magnitude [?].

The strategy consists in writing down the Lorentz force (eq. 27) and solving [?]:

$$\frac{\vec{v}_{n+\frac{1}{2}} - \vec{v}_{n-\frac{1}{2}}}{\Delta t} = \frac{q}{m} \frac{\vec{v}_{n+\frac{1}{2}} + \vec{v}_{n-\frac{1}{2}}}{2} \times \vec{B} \,, \tag{120}$$

and

$$\frac{\vec{r}_{n+1} - \vec{r}_n}{\Delta t} = \vec{v}_{n+\frac{1}{2}} \,. \tag{121}$$

Here n denotes the step at which the equation is being solved. It is clear that this scheme offsets velocity and position by half a step with respect to each other.

One can define $v_+ \equiv v_{n+\frac{1}{2}}$ and $v_- \equiv v_{n-\frac{1}{2}}$. Equation 120 then becomes [?]

$$\frac{\vec{v}_+ - \vec{v}_-}{\Delta t} = \frac{q}{2m} (\vec{v}_+ + \vec{v}_-) \times \vec{B} \,. \tag{122}$$

This equation seems like a rotation, and indeed it is. The velocity vector will rotate by an angle Θ, with a corresponding vector

$$\vec{u} = -\frac{\vec{B}}{|\vec{B}|} \tan\left(\frac{\Theta}{2}\right) \,. \tag{123}$$

This rotation will occur about

$$\vec{v}' = \vec{v}_- + \vec{v}_- \times \vec{u} \,, \tag{124}$$

which is perpendicular both to the magnetic field and the vector $\vec{v}_+ \pm \vec{v}_-$.

The velocity at the end of the step can now be written as

$$\vec{v}_+ = \vec{v}_- + \vec{v}' \times \vec{w} \,, \tag{125}$$

where a new vector ($\vec{w}$) was introduced [?]:

$$\vec{w} = \frac{2\vec{u}}{1 + |\vec{u}|^2} \,. \tag{126}$$

The strategy outlined above is applied successively to each step.

One of the main advantages of employing BP over CK is the fact that it is energy-conserving. Moreover, in the usual RK schemes errors tend to accumulate, whereas for BP they tend to average out. Finally, the BP algorithm would works efficiently also in the presence of electric fields, since eq. 122 would retain the same form and only $\vec{v}_{\pm}$ would change.

3.2.3 Solving the Fokker-Planck transport equation

See ref. [**?**].

3.3 Modelling the transport of astroparticles

Particle transport refers to the strategies to describe the intricacies of the motions of particles in various media. Strategies to perform this modelling in the context of (high-energy) astrophysics and astroparticle physics will be presented in this section, applied to the case of CR nuclei, gamma rays, and neutrinos.

Two main strategies have been used to simulate the propagation of astroparticle in diverse environments, transport equations and Monte Carlo (MC) methods, described in §3.3.1 and §3.3.2, respectively.

3.3.1 Transport equations

Analytical and semi-analytical methods to solve particle interactions have been widely used for decades, given their relative simplicity. They are usually fast and rely on the solution of several integrals over an ensemble of particles (as opposed to the Monte Carlo approach which does this on a particle-by-particle basis, as described in §3.3.2).

While fast, transport equations are not applicable to all cases. For instance, these methods are not adequate for three-dimensional studies involving magnetic deflections, which is commonly the case in astroparticle physics. They also come short in the treatment of some stochastic processes that yield copious amounts of different by-products, such as photodisintegration (see §2.7.3).

Consider a distribution of charged particles of type a with density $n(\vec{r}, t, E)$. Suppose that other particles b can, due to some interaction, convert into a. The general form of the transport equation for particle a is:

$$\frac{\partial n_a(\vec{r}, \vec{p}, t)}{\partial t} + F_{\text{diff}}(\vec{r}, \vec{p}, t) + F_{\text{int}}(\vec{r}, \vec{p}, t) + F_{\text{dec}}(\vec{r}, \vec{p}, t) + F_{\text{cel}}(\vec{r}, \vec{p}, t) + F_{b \to a}(\vec{r}, \vec{p}, t) = Q(\vec{r}, \vec{p}, t) \tag{127}$$

where $\vec{r}$ is the position, t is the time, $\vec{p}$ is the particle's momentum, and Q is a source term. This equation describes how a density of particles of type a evolve. The F_{diff} term describes spatial diffusion of this ensemble of particles considering a diffusion coefficient D (see §2.5.4.3 for details). It reads

$$F_{\text{diff}}(\vec{r}, \vec{p}, t) = -\vec{\nabla} \left[D(\vec{r}, t) \vec{\nabla} n_a(\vec{r}, \vec{p}, t) \right] . \tag{128}$$

F_{int} describes changes in the particle density due to spurious interactions:

$$F_{\text{int}}(\vec{r}, \vec{p}, t) = \sum_{t=\{\text{targets}\}} v m_t \sigma_{\text{at}}(E) n_t(\vec{r}, \vec{p}, t) n_a(\vec{r}, \vec{p}, t) , \tag{129}$$

where $\sigma_{\text{ine}}(E)$ is the total inelastic cross section (see §2.1.2) for particles of type a and energy E, m_t is the mass of the target particles, and n_t their number density. The term F_{dec} describes possible decays of the particles of interest, if they have a finite lifetime, i.e., if $\tau_a < \infty$, it reads:

$$F_{\text{dec}}(\vec{r}, \vec{p}, t) = -\frac{\gamma}{\tau_a} n_a(\vec{r}, \vec{p}, t) \,. \tag{130}$$

Continuous energy losses are included in the equation through F_{cel}, which is given by

$$F_{\text{cel}}(\vec{r}, \vec{p}, t) = \frac{\partial}{\partial E} \left(\left| \frac{\mathrm{d}E}{\mathrm{d}t} \right| n_a(\vec{r}, \vec{p}, t) \right) \,. \tag{131}$$

The transport equation given by 127 is for particle a exclusively. However, other particles have to be modelled likewise, which might end up producing particles of type a. This is accounted by $F_{b \to a}$:

$$F_{\text{b}\to\text{a}}(\vec{r}, \vec{p}, t) = -\sum_{b=\{\text{others}\}} \left[\int_E^\infty \mathrm{d}E_b \, \frac{\mathrm{d}\sigma\,ab(E, E_b)}{\mathrm{d}E} n_b(\vec{r}, \vec{p}, t) \right] n_a(\vec{r}, \vec{p}, t) \,. \tag{132}$$

The actual equation to be solved is the system of N_a equations like this. If nuclei are involved, this can get increasingly complicated because the system of equations would include all isotopes being created via, e.g., photodisintegration and spallation.

Note that the term F_{diff} includes spatial diffusion due to magnetic fields. This makes the problem more difficult to be treated and is often neglected. However, it may be important even in this one-dimensional treatment, since it is responsible for accounting for magnetic horizon effects [**?** **?** **?**]

Only in some particular cases can eq. 127 be solved analytically. This is the case of the **leaky box model** for GCRs. In the general case some strategies have to be devised. One possibility is to transform the system of differential equations for all particles, given by eq. 127, into a vector-like expression of the form:

$$\frac{\partial}{\partial t}\vec{\mathcal{N}}(\vec{r}, t, E) = \overleftrightarrow{\Gamma} \cdot \vec{\mathcal{N}}(\vec{r}, t, E) + \vec{Q}(\vec{r}, t, E) \,, \tag{133}$$

where $\vec{\mathcal{N}}$ is

$$\vec{\mathcal{N}}^T \equiv\!= (n_{a_1,b_1} \dots n_{a_1,b_m} \dots n_{a_n,b_1} \dots n_{a_n,b_m}) \,, \tag{134}$$

with the superscript T denoting the transpose of the vector. Note that here a simplification was made. The phase space was reduced to $\vec{r}, E, t$ instead of $\vec{r}, \vec{p}, t$.

The matrix $\overleftrightarrow{\Gamma}$ encapsulates interactions and energy losses, and $\vec{Q}$ is the source term for each type of particle. $\overleftrightarrow{\mathcal{P}}$ can be interpreted essentially as a matrix containing rates and informing whether one particle generated another that should be accounted for in its corresponding (coupled) equation. The solution can be obtained by computing a grid of energies and rates, as well as combinations of correlated processes. Each energy bin k has width $\Delta E_{k+1} = E_{k+1} - E_k$. The equation is solved for each of these bins. A corresponding distance step (actually time) is also chosen, such that the final result is the sum over these steps.

The algorithm briefly alluded to above is used, for example, in the `PriNCe` code [**?** **?**] for UHECR propagation. Similar idea is employed in the TransportCR code [**?**]. A code for high-energy gamma-ray and electron transport called DINT [**?**] also employs a similar idea.

These methods can only be applied to the one-dimensional case, not being suitable for the more general three-dimensional with magnetic-field effects when directional dependence is required. That is when MC methods come in handy.

3.3.2 Monte Carlo methods

Monte Carlo *methods* refer to a class of algorithms that make use of random numbers to solve a particular problem. MC *simulations* make use of sampling to obtain the statistical behaviour of a system or phenomenon.

MC uses (pseudo-)random numbers. A pseudo-random number generator (PRNG) takes as input some initial arbitrary value (called *seed*) and use some algorithm to obtain a seemingly random distribution of numbers. The use of seeds allow for reproducibility. For details on how this works, see appendix A.

For particle transport MC methods consist in solving the equations of motion of a particle within tiny steps including changes in momentum due to, e.g., magnetic deflections, as well as particle interactions. This is done probabilistically, on a particle-by-particle basis. The step size is an important parameter that determines both the accuracy and the speed of the simulation. Variable step sizes are desirable if the processes being investigated have a large dynamical range.

This strategy for astroparticle propagation can be split into two parts. The first consists in solving the equation of motion, *without interactions*, within a step. In the presence of magnetic fields and no interactions, this would mean solving eq. 27. The second part is the treatment of interactions. For continuous energy losses the particle being propagated loses an amount of energy of

$$\Delta E = \left| \frac{\mathrm{d}E}{\mathrm{d}x} \right| \Delta x \,, \tag{135}$$

where Δx is the step size. For stochastic processes, common algorithms sample from an exponential distribution based on the mean free path (λ). For instance, a decision on whether the interaction occurs or not depends on a random number drawn ($0 \leq r < 1$). If

$$\Delta x > -\log(r)\lambda \,, \tag{136}$$

then an interaction takes place. Otherwise, it is important to check whether the step is sufficiently large to resolve the interaction of interest. In case it is too large, then the next step should be reduced according to some desired tolerance.

If secondaries are produced in an interaction or due to a continuous energy-loss process, they are sampled from distributions. There are a few MC methods that facilitate that, described in appendix B. The optimal choice generally requires considerations about convergence speed, which ensures that the distribution is quickly retrieved for a sample of a given size.

3.3.3 Codes for astroparticle propagation

Several simulation codes exist for the propagation of astroparticles in the universe. Some are transport-equation solvers, others perform Monte Carlo simulations.

For UHECRs the main codes are listed in table 3.3.3. Note that they all store secondary particles produced in the interactions, like gamma rays, electrons, and neutrinos, but except for CRPropa they do not perform the propagation of these particles. That would require external tools.

Table 2: List of simulation codes for UHECR propagation. The type of treatment of the code, Monte Carlo (MC) or using transport equations (TE) are indicated.

code	dimensions	approach	references
CRPropa	1D, 3D	MC	[? ? ? ? ? ?]
SimProp	1D	MC	[? ?]
PriNCe	1D	TE	[?]
TransportCR	1D	TE	[?]

There are also codes dedicated to the transport of "lower-energy" CRs, this is, those that are not UHECRs. These are mainly GCRs, with energies below ~ 100 PeV [? ?]. The propagation of CRs in environments other than the Galaxy, like galaxy clusters [? ? ? ?], is also described by the same underlying theory and similar computational tools could be used. Some of the existing codes are listed in table 3.3.3.

Table 3: List of simulation codes for GCR propagation. The type of treatment of the code, Monte Carlo (MC), employing grid-based transport equations (TE), or using stochastic differential equations (SDE) is indicated.

code	approach	references
CRPropa	SDE	[? ? ? ? ? ?]
GALPROP	TE	[? ?]
DRAGON	TE	[? ? ?]
PICARD	TE	[?]

Codes for gamma-ray propagation usually treat both gamma rays and electrons. Besides the approach to solving the transport (Monte Carlo vs. transport equations), these softwares differ in the energy range at which they operate. Table 3.3.3 present some of them.

Table 4: List of simulation codes for gamma-ray propagation. They also include the treatment of electron-photon interactions. The type of treatment of the code, Monte Carlo (MC) or transport equations (TE) is indicated, together with the dimensionality of the treatment (1D or 3D). If the code is only suitable for UHE ($E \gtrsim 1 - 10$ PeV), this information is also provided.

code	dimensions	$E < E_{\text{UHE}}$	$E > E_{\text{UHE}}$	approach	references
CRPropa	1D, 3D	✓	✓	MC	[? ? ? ? ? ?]
Elmag	1D, 3D	✓		MC	[? ? ?]
DINT	1D	✓	✓	TE	[?]
CECsi	1D, 3D	✓		MC	[?]
EleCa	1D		✓	MC	[?]
γ-cascade	1D	✓		TE	[?]

In §4 the CRPropa framework will be described.

4   The CRPropa framework

CRPropa was devised to simulate the propagation of high-energy particles. It was initially conceived to study UHECRs [? ?], but thanks to its modular design nowadays it can also perform the transport of other particles such as electrons, photons, and neutrinos. However, it is still limited to *ultrarelativistic* particles, since it approximates velocities by the speed of light.

Given its widespread adoption by the CR and gamma-ray communities, CRPropa is the tool that will be taught as part of this course. In §4.1 I provide a technical overview of the code. Sections §4.2, §4.3, §4.5, and §4.7 describe some of the basic ingredients required to build a simulation. Comments about the analysis of the outputs at post-processing stage can be found in §4.8, together with some example simulations in §**??**.

4.1 Overview

CRPropa 3 [**? ? ? ?**] is written in C++. It is a significant leap forward with respect to the previous version. It interfaces with Python through SWIG [12]. This enables users to directly access all of the code's functionalities directly from Python, while capitalising on the performance of C++. SWIG also enables cross-language polymorphism, enabling users to create code extensions in Python that directly interacts with the core C++ library.

CRPropa runs in parallel with shared memory using OpenMP[13]. This guarantees that some simulation ingredients like matter and magnetic-field distributions are committed to memory only once, while different threads split the job of performing the transport of particles. Moreover, only one instance of each module is loaded, since all modules are stateless.

All particles in CRPropa are passive objects of type `Candidate`, which are the particles. They hold information of the physical state of the particle, as well as some other auxiliary information such as step sizes, and flags referring to the particle state (e.g., `isActive`). Stateless modules act on candidates and change their properties at each step of propagation.

The `ModuleList` is the central engine of CRPropa. It contains the `Module` objects that effectively act on the candidates. A loop over the module list, together with successive iterations of the candidates until a break condition is met, are responsible for the propagation. The internal flag `isActive` is responsible for deciding whether a given candidate will be processed by the modules in the list. An overview of the code structure is presented in fig. 7.

4.2 Sources

Values can be assigned to the particles (or *candidates*) in two ways. The first is by explicitly setting all properties such as initial redshift, momentum, energy, particle type, position, etc. The second is by randomly drawing this values from some distributions, by considering a `Source` object. `Source` encapsulates all relevant details to fully characterise a candidate via a `SourceFeature`, which can be added directly to it via the `add` method.

The type of particle is assigned to the candidate using the features below.
- `SourceParticleType`: assigns a single type of particle to the candidate.
- `SourceMultipleParticleTypes`: draw the type of particle from a distribution according to their relative weights.

The energy distribution can be ascribed to the candidate in various ways, listed below.
- `SourceEnergy`: attribute the same energy to all candidates.
- `SourcePowerLawSpectrum`: randomly select the candidate's energy from a power-law distribution with a given spectral index α, for $E_{\mathrm{min}} \leq E \leq E_{\mathrm{max}}$.

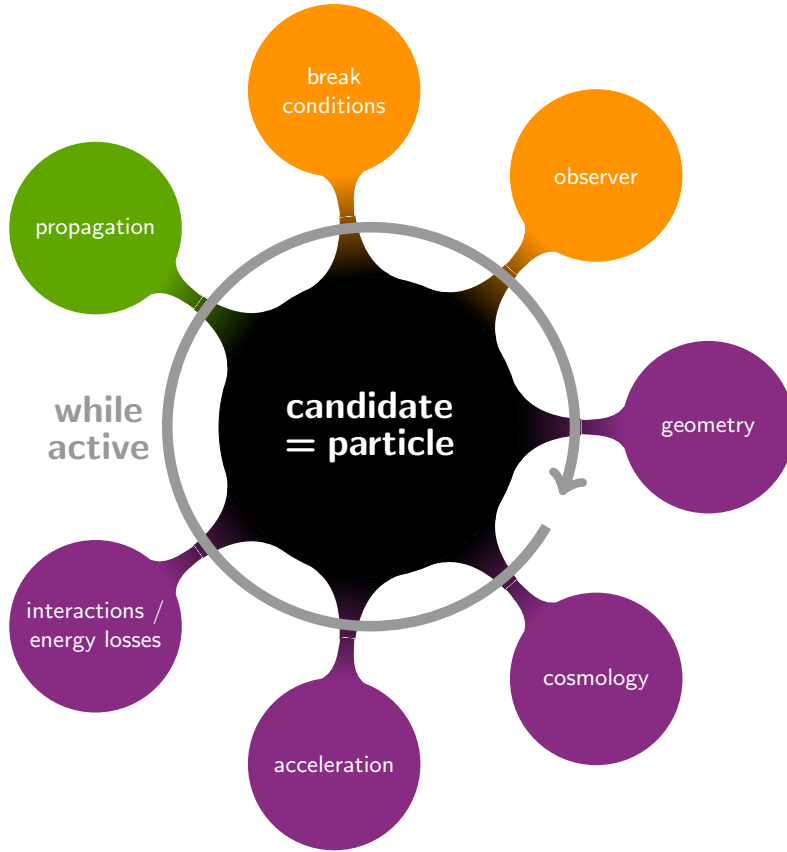[12] www.swig.org
[13] www.openmp.org

Figure 7: Scheme illustrating CRPropa's modular structure. Each module contained in the module list acts on a particle (`Candidate` object). The candidate is propagated while its state is flagged active, which is controlled by observer and break conditions. These checks are performed at each cycle of the module list.

- `SourceComposition`: this is the same as `SourcePowerLawSpectrum` but considering a maximum rigidity (R_{max}) for the particles, instead of a maximum energy (E_{max}). It also specifies the composition and its relative abundance, rendering `SourceMultipleParticleTypes` and `SourceParticleType` redundant.

   The spatial distribution of sources is arguably one of the most important aspects of modelling, given its evident impact on any analysis. Therefore, an extensive list of tools to attribute source positions to candidates is available, some of which are shown below.

- `SourcePosition`: specifies the position vector (`Vector3d`) of a source.
- `SourceMultiplePositions`: randomly selects position vectors from a list of positions representing individual sources, which can have different weights (luminosity).
- `SourceUniform1D`: randomly draws the distance of a source from a uniform distribution and assigns it to the x-coordinate of the position vector.
- `SourceUniformSphere`: the initial position vector of the candidate is taken from a uniform distribution within a spherical volume.
- `SourceUniformShell`: position vectors are randomly chosen somewhere on the surface of a sphere of a given radius.
- `SourceUniformHollowSphere`: the position vectors are chosen uniformly in the volume of the gap between two spherical shells.

- SourceUniformBox: same as SourceUniformSphere, but considering the volume of a cube instead of a sphere.
- SourceUniformCylinder: same as SourceUniformSphere, but considering the volume of a cylinder instead of a sphere.
- SourceSNRDistribution: the position vector of the candidate is randomly assigned following the distribution of supernova remnants in the Milky Way, according to ref. [**?**].
- SourcePulsarDistribution: this provides the spatial distribution of pulsars in the Galaxy according to ref. [], with an additional improvement in the radial component owing to ref. [**?**].
- SourceDensityGrid: randomly draws the source position from a grid in which each cell describes the relative probability of that region with respect to all the others.
- SourceDensityGrid1D: same as SourceDensityGrid, but only the x-coordinate of the position vectors are attributed to the candidate.

In more advanced simulations like the three-dimensional case, the initial direction of the candidate has to be carefully selected considering that it determines the arrival directions. A list of available resources is shown below.
- SourceDirection: specify the (normalised) vector describing the direction of motion of a particle.
- SourceIsotropicEmission: the emission direction is randomly chosen assuming equal probabilities in all directions.
- SourceEmissionCone: the emission vector is chosen randomly within a given angle around a reference direction.
- SourceDirectedEmission: the emission direction is drawn from a von-Mises–Fisher distribution. This is particularly useful for the targeting method to speed up three-dimensional simulations, described in ref. [**?**].

To specify the redshift of a candidate, several functionalities are available, as described below.
- SourceRedshift: a fixed initial redshift is assigned to a candidate.
- SourceUniformRedshift: draws the initial redshift from a uniform distribution within a given interval.
- SourceRedshiftEvolution: the redshift of the candidate is randomly chosen from a power-law distribution within a given redshift interval, according to $(1+z)^m$, wherein m is a constant.

For more details on the treatment of cosmological effects within CRPropa, see 4.6.

4.3 Observers

So far it has become clear that CRPropa can be used as an event generator mimicking astrophysical sources of high-energy particles. These particles can then be tracked. But *how do we mimic a real-word detection?* For that we can use an object of type Observer, which acts as a detector of sorts. It serves as a geometrical breaking condition that enable some actions to be triggered when a candidate crosses its boundary (i.e., upon detection). One such action is to store the candidate information, saving it to a file.

For an Observer, particles can have one of three states: NOTHING, DETECTED, VETO. All candidates are in the former state until an ObserverFeature changes it.

An observer can be omnipresent, detecting all particles everywhere at all times. This is what

`ObserverDetectAll` does. However, this is not always practical considering the amount of information to be stored, the bulk of which are seldom useful. For this reason, it is often convenient to define the observer as a spatial object, with a corresponding geometry (e.g., sphere, cube, plane, etc). This is exactly what `ObserverSurface` does. It flags as `DETECTED` a particle that crossed the surface boundary.

`Observer1D` is a specific type of observer suitable for one-dimensional simulations. It detects particles when they reach $x = 0$, neglecting the other components of the candidate's position vector.

In some cases users might want to simply ignore some particles that are actually detected by an observer. For instance, the study requires information of only photons and not electrons, of neutrinos and not nuclei. In this case, the state `VETO` is assigned to candidates that are detected. There are several types of vetoes to ignore specific types of particles. They can all be added to the same observer. `ObserverNucleusVeto` changes the state of *detected* atomic nuclei to `VETO`. The same is done by `ObserverNeutrinoVeto`, `ObserverPhotonVeto`, and `ObserverElectronVeto`. For other types of particles, `ObserverParticleIdVeto` vetoes all particles with a specific particle id.

An observer need not be a purely spatial geometrical object. It can also be time-dependent. This is the case of `ObserverRedshiftWindow`, which flags as `DETECTED` candidates that arrive with redshift between z_{min} and z_{max}, provided by the user.

When the time evolution of a particle density is needed, `ObserverTimeEvolution` detects candidates in arbitrary (linearly or logarithmically spaced, or custom) time intervals. It also limits the size of the next step to prevent overshooting of the time windows. This is particularly useful for the propagation of GCRs.

Reaching the observer is a natural breaking condition: once a candidate is detected, there is no longer a need to keep tracking it. However, sometimes it is useful to keep them active, as in the case of multiple observers concomitantly acting upon particles in a single simulation. In this case, the observer has to be instructed to keep the candidate active even after detection. This is achieved with the method `setDeactivateOnDetection(False)`.

An `Observer` can dump information of all candidates into a file. This can be done using the method `onDetection(output)`. Here output is an object indicating the type of output that will be stored: `ShellOutput` (print to the shell), `TextOutput`, `HDF5Output`. Another possibility is to use a `ParticleCollector`, which is a temporary memory buffer that stores particle information for later internal usage.

4.4 Propagation modules

Four modes of propagation are available in CRPropa.

`SimplePropagation` is the simplest mode of propagation, suitable for one-dimensional applications or whenever magnetic deflections can be ignored. At each step k of size Δx_k, it does computes $\vec{r}_{k+1} = \vec{r}_k + \Delta x_k \hat{p}$, where $\vec{r}_k$ is the position vector at the k-th step, and $\hat{p}$ is the normalised momentum.

Whenever one requires to resolve trajectories subject to a Lorentz force, `PropagationCK` is a suitable option. This three-dimensional propagation implements an adaptative Runge-Kutta algorithm, described in §3.2.1, with Cash-Karp coefficients [**?**].

A new feature implemented in CRPropa 3.2 [**?**] is the Boris push algorithm, already described in §3.2.2 through the `PropagationBP` module. This is currently the recommend algorithm recommended by the CRPropa Developers.

4.5 Break conditions

Break conditions are an essential part of the algorithm, constituting the stopping criterion for the simulation. In their absence, the simulation would go on indefinitely. The state of a candidate is changed from `active` to `inactive` when it meets a break condition.

A candidate will no longer be tracked by the code if at least one of these conditions are met:

- `MaximumTrajectoryLength`: the trajectory length described by this particle is too large;
- `MinimumEnergy`: the candidate's energy dropped below a given threshold;
- `MinimumRigidity`: its rigidity dropped below a given threshold;
- `MinimumRedshift`: the redshift of the candidate is smaller than a threshold value;
- `MinimumChargeNumber`: the candidate has a charge[14] smaller than a given value.

The list above is not exhaustive. For more details, see CRPropa's documentation.

4.6 Cosmology

CRPropa implements the usual concordance Λcold dark matter (CDM) cosmological model. The default cosmological parameters inferred by the Planck satellite [**?**], but this can be changed by the user.

Internally, the code treats distances as comoving, by default. To enable fast conversion between distance measures (e.g., comoving, light-travel, luminosity), simple interpolations are performed for values in the range $10^{-4} < z < 100$, spaced logarithmically.

In CRPropa, redshift (z) is used as a measure of time through equation 106. This quantity can be optionally used for various purposes. It can be attribute to a candidate by using the corresponding source features.

Because redshift is a measure of *time*, as opposed to *distance*, a source at a given distance D will only have a redshift z that corresponds to this distance, following eq. 106, if the simulation is one-dimensional and time delays incurred by magnetic fields are absent.

Adiabatic energy losses due to the expansion of the universe are implemented in the `Redshift` module. Note that the notion of negative redshift is allowed within the code through `FutureRedshift`, making it possible to treat $z < 0$. Physically this would translate into a future observation of the particle.

4.7 Particle interactions and decays

The interaction modules implement physical interactions between particles. They decide whether the kinematic state of a particle changes at a given time, and can also produce secondary particles. Two types of algorithms are employed, depending on the interaction. Some processes are described in the continuous energy-loss approximation (§3.3.1) for performance reasons, whereas for others a full Monte Carlo approach is used, as described in §3.3.2.

Interaction processes in CRPropa rely on pre-computed interaction rate tables. The scripts for their calculation can be seen in the CRPropa3-data repository[15]. These tables are automatically download when CRPropa is installed.

Stochastic interactions modelled through a Monte Carlo approach are treated as follows. At each step the interaction rate, or conversely the interaction length (λ), for a candidate of energy E is read

---

[14]Actually, it is not the charge but the atomic number of a cosmic ray.
[15]https://github.com/CRPropa/CRPropa3-data

from the look-up tables. The probability that the particle will not undergo an interaction is decided, following the description from §3.3.2.

One important aspect of the interaction modules is that the modules limit the size of the next propagation step to ensure that the process is properly resolved in space. This means that wherever interaction rates are larger, step sizes are smaller. The user can choose the tolerance above which the size of the next step will be limited. The default value is 10% for the ratio between the current step size and the interaction length. For the continuous energy-loss processes, the energy loss is simply $\Delta E = \mathrm{d}E/\mathrm{d}x\,\Delta x$, where $\mathrm{d}E/\mathrm{d}x$ is theoretically known, and Δx is the step size. Similarly to the stochastic processes, the next step is also limited according to the same criteria.

CRPropa contains a list of pre-implemented interactions. They are generally sufficient to describe the propagation of UHECRs, gamma rays, and electrons over cosmological distances. Extragalactic background radiation fields from the CMB, EBL, and CRB are implemented by default (see §2.4.1). Custom isotropic radiation fields can also be implemented by the user. The interactions currently implemented are shown in figure 8.
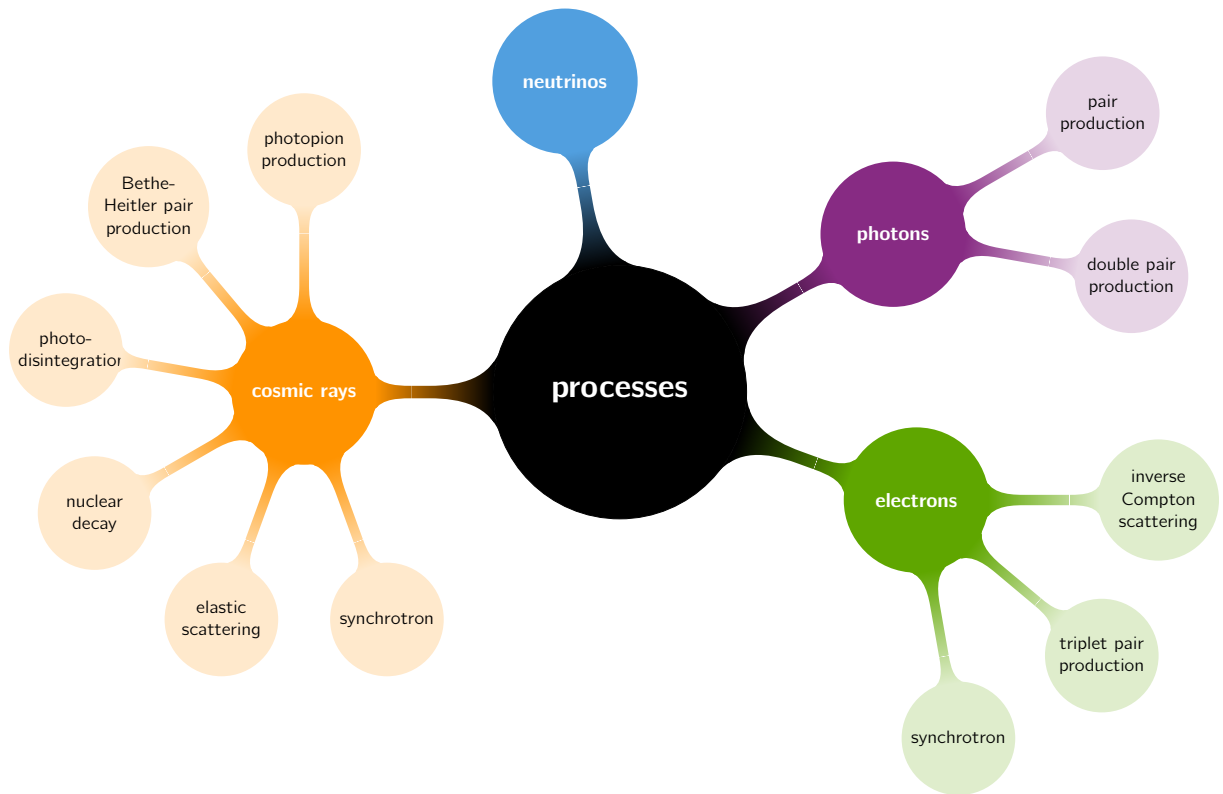

Figure 8: Diagram describing the interactions and energy-loss processes implemented in CRPropa, for different types of particles. Figure taken from ref. [**?**].

Below the implemented interactions are described. The underlying details of these processes are described in §2, from a theoretical viewpoint.

4.7.1 Photopion production

The production of mesons due to photonuclear interactions is described in §2.7.2. The most important of these processes for most applications is *photopion production*.

CRPropa uses the SOPHIA [**?** **?**] event generator to model the interaction between nucleons

(protons and neutrons) and photons. The cross section for this is shown in fig. 6. In the case of nuclei, the mean free path is approximated as a superposition of those for protons (λ_p) and for neutrons (λ_p):

$$\lambda(E) \approx 1.18 \left[Z^a \lambda_p^{-1} \left(\frac{E}{A} \right) + N^a + \lambda_n^{-1} \left(\frac{E}{A} \right) \right]^{-1}, \tag{137}$$

where $N = A - Z$ is the number of neutrons in the nucleus, and $a = 2/3$ if $A \leq 8$ or $a = 1$ otherwise. This approximation neglects the Fermi motion within the nucleus. It also does not take into account possible spectral changes in the resonances. However, it leads to errors smaller than $\sim 20\%$ for UHECR propagation [?].

4.7.2 Bethe-Heitler pair production

This process, described in §2.7.1, is implemented in the continuous energy-loss approximation. For nuclei, the energy-loss length is scaled with respect to that of protons:

$$\left[\frac{1}{E} \frac{dE}{dx} \right]_{^A_Z X} = \frac{Z^2}{A} \left[\frac{1}{E} \frac{dE}{dx} \right]_p. \tag{138}$$

4.7.3 Photodisintegration

The first versions of CRPropa [?] prior to 1.3 did not allow for the propagation of nuclei. This was implemented later [? ?], and released with CRPropa 2 [?]. The underlying theory is described in §2.7.3.

Cross sections for this process are taken from multiple sources. For nuclei with $A < 12$, the sources and details are listed in table 5.

Table 5: References for the photodisintegration cross sections for nuclei with $A < 12$. Table adapted from ref. [?].

nucleus	reference	details
^{2}H	[?]	
^{3}H	[?]	rescaled by factor 1.7
^{3}He	[?]	rescaled by factor 0.66
^{4}H	[?]	
^{7}Li	[? ?]	interpolation of measured data
^{8}Li	[?]	loss of neutron
^{9}Li	[?]	loss of neutron
^{7}Be	[?]	loss of proton
^{9}Be	[? ?]	parametrization from [?], refitted with data from [?]
^{10}Be	[?]	loss of neutron
^{11}Be	[?]	loss of neutron
^{8}B	[?]	loss of proton
^{10}B	[?]	loss of neutron and proton
^{11}B	[?]	loss of neutron
^{9}C	[?]	loss of proton
^{10}C	[?]	loss of proton
^{11}C	[?]	loss of proton

For $A \geq 12$, photonuclear cross sections are retrieved from the TALYS code [? ? ? ?], in

particular version 1.8 (for CRPropa 3.2).

Based on the individual exclusive cross sections computed, it is possible to obtain the number of channels for each nucleus-photon interaction and the total cross sections. To reduce the number of channels and therefore the memory requirements of the code, only channels that contribute with at least 1% to the total cross section are considered; the others are discarded.

4.7.4   Nuclear decay

Nuclear decay modules in CRPropa include alpha, beta, and gamma decays, as well as neutron and proton dripping (see §2.6).

In CRPropa the treatment of nuclear decays is based on tabulated values obtained from the NuDat 2.6 database [**?** **?**], which provides data for nuclear lifetimes as well as number of decay channels.

4.7.5   Elastic scattering

Being an important channel for the production of photons, elastic scattering (see §2.7.4) has been recently incorporated into CRPropa [**?** **?**] and released with CRPropa 3.2 [**?**]. A more detailed theoretical description of this process is given in §2.7.4.

The cross sections for this process are also extracted from the TALYS code, like those for photo-disintegration. It would be computationally expensive to build and load tables relating the outgoing photon energy to the primary nucleus energy for all photon backgrounds. Therefore, to reduce memory consumption the average cross section for all isotopes of a given element is computed and scaled by a factor $Z(A - Z)/A$.

The energy of the background photon scattered by the nucleus has a probability distribution function (PDF) given by [**?**]:

$$p\left(\gamma, \varepsilon'\right) = \frac{\mathrm{d}\lambda^{-1}\left(\gamma, \varepsilon'\right)}{\mathrm{d}\varepsilon'} \, , \tag{139}$$

where γ is the Lorentz factor of the nucleus and ε' is the energy of the photon in the nucleus rest frame. The cumulative distribution function (CDF) obtained from this PDF is provided as look-up table, and by using inversion sampling the energy of the up-scattered photon can be retrieved, followed by a Lorentz boost to transform it back to the laboratory frame.

4.7.6   Electromagnetic interactions

Electromagnetic processes of the type $X + \gamma_{\mathrm{bg}}$, where $X = \{\gamma, e^+, e^-\}$ are implemented in CRPropa in a similar way. They are:
- Breit-Wheeler pair production (see §2.9.1);
- inverse Compton scattering (see §2.9.2);
- double pair production (see §2.9.3);
- triplet pair production (see §2.9.4).

All of these load interaction rate tables for each background photon field to determine whether the interaction will happen.

The energies of the particles produced are interpolated from look-up tables containing tabulated the PDF corresponding to the differential interaction rates. This allows for the sampling of the energy fractions taken by each of the final particles.

Starting off with a (high-energy) photon, successive pair production and inverse Compton interactions create an electromagnetic cascade. For each pair production, two particles are created, one electron and one positron. Therefore, the total number of particles would increase as 2^N, wherein N is the number of interactions taking place. For this reason, a **thinning** procedure was implemented, inspired by ref. [**?**].

Suppose a secondary particle produced through these processes carries a fraction y of the energy of the primary. The thinning algorithm draws a random number (r) and decides whether or not to accept this particle. For a thinning parameter η, with $\eta \in [0, 1]$, if $r < (1 - y)^\eta$, the particle continues to be tracked; otherwise it is inactivated. For $\eta = 0$ there is no thinning, whereas for $\eta = 1$ this weighted sampling is maximum. If the particle is accepted, its weighted is updated by a factor $y^{-\eta}$. Note that these weights should be taken into account in the post-processing (see §4.8) of the simulations. η should be chosen according to the problem at hand, to maximise both performance and accuracy for a finite-sized sample.

4.7.7 Synchrotron emission

The energy-loss length for synchrotron emission is described in §2.11.1 through eq. 99. In CRPropa this is implemented as a continuous energy-loss process. At each step, the magnetic field ($\vec{B}$) is evaluated at its centre. After propagating a small distance Δx corresponding to the step size, at the end of the step the charged particle will have lost an amount of energy $\Delta E = |dE/dx|\Delta x$.

The synchrotron radiation emitted has to add up to the total energy budget available, ΔE. Its spectrum is given in §2.11.1, considering the asymptotic limit, wherein $F(y) \gg G(y)$ (see eqs. 101 and 102).

While CRPropa can treat this process, if individual synchrotron photons are added and later propagated, memory overflows are expected due to the copious amounts of these particles produced at each step.

4.8 Postprocessing the simulations

A Random number generators

Pseudo-random number generators (PRNGs) are a class of algorithms for generating a sequence of numbers that, collectively, resemble a sequence of random numbers. They started to be required for computational applications in the late 1940s [**?**].

Sequences generated by PRNGs are not truly random. The **seed**, which is the initial value provided, completely *determines* the whole sequence of numbers. This sequence starts to repeat itself after a given **period**, which depends on the details of the PRNG algorithm being employed. Therefore, PRNGs are *deterministic*, in the sense that for a fixed seed the same sequence of numbers can be generated, and *periodic*, which means that the sequence will eventually repeat itself.

In §A.1 one of the arguably simplest PRNG is presented. §A.2 describes a widely use algorithm, the Mersenne Twister.

A.1 Linear congruential generator

The linear congruential generator (LCG) is one of the simplest PRNG algorithms available. The k-th number of the sequence (x_k) is generated based on the previous ones, considering the initial value

x_0 (the *seed*). They are defined through the recurrence relation

$$x_{k+1} = (ax_k + b) \mod m, \tag{140}$$

where a $(0 < a < m)$ is the multiplier, b $(0 \leq b < m)$ is the increment, and m $(m > 0)$ is the modulus, which is the remainder of a division between any two numbers.

The first LCG was a multiplicative congruential generator, with $b = 0$ in eq. 140 [?]. The more general form expressed by this equation was published a few years thereafter [? ?].

A.2   Mersenne twister

Mersenne twister (MT) is a well-known algorithm for generating (pseudo-)random numbers [?]. Historically, it was motivated due to the limitations of earlier PRNGs.

MT is a fast generator with period chosen to be a Mersenne prime, of the form $2^N - 1$. In the most common implementation, MT19937, $N = 19937$, for a 32-bit word length. There are also 64-bit versions.

This algorithm is excessively complex to be briefly summarised here. The interest readers are referred to

B   Monte Carlo sampling methods

Inversion sampling is arguably the simplest algorithm. For a distribution $(f(x))$ corresponding to the PDF of a function, it is straightforward to compute the CDF $(F(x))$. Then a random number (r) is generated. Since both $F(x)$ and r have the same domain, a sample of x can be obtained: $x = F^{-1}(r)$. The main disadvantage of this method is that very few distributions possess CDF whose inverse can be easily and efficiently evaluated.

Another commonly used method is **rejection sampling**. It relies on creating a proposal function $g(x)$. A pair of random number (r_x, r_g) is uniformly drawn for a given range of interest. A sampled value of x is accepted if $r_g < f(r_x)$. Depending on the shape of the proposal function $g(x)$, this can lead to long computational times.

Importance sampling is a generally more robust sampling strategy. It relies on reweighting the desired distribution $f(x)$ with a given function $w(x)$, as follows:

$$f(x)\mathrm{d}x = \frac{f(x)}{w(x)} w(x)\mathrm{d}x. \tag{141}$$

This means that a sample is drawn from a proposal distribution and reweighted to attribute higher weights to values that are more typical, but using a function that is easier to sample.